We thank the anonymous reviewer #1 for the helpful comments. These comments helped to substantially improve the manuscript. Below we give detailed answers to the individual reviewer comments in blue.

This study provides some nice laboratory measurements which can be used to infer the surface texture of ice crystals. However, the manuscript in its present form needs some improvements in terms of clarity. Jargons are used to introduce some parameters, but the physical meanings of these parameters are not clearly explained. It is challenging to apply the results/findings of this study to the simulation of the optical properties of ice crystals in a straightforward manner. Below are some specific comments for the authors' consideration in the revision process.

1) On page 9, the physical meaning of the parameter known as "combined roughness measure" or "the normalized energy feature parameter ke" is difficult to understand, even after repeated reading (including reading Appendix A). The authors cited Lu et al. (2006) for the definition of ke. In the revised manuscript, would it be possible to give a clear physical meaning of this parameter?

We agree with the reviewer that the physical meaning of these roughness parameters is difficult to understand. Therefore, we significantly revised Section 2.1.2 of the manuscript by explaining in details how the roughness parameter k_e is calculated from the SID-3 scattering patterns and what the parameter values mean in terms of a physical roughness.

2) In Table A1, "energy" and "combined roughness" are used. What exactly are the "energy" and "combined roughness" here?

These terms are now clearly defined in Section 2.1.2 of the revised manuscript.

3) On page 9 and in Figure B1, the reviewer does not understand the motivation to correlate the parameter "sigma" and ke. Here the sigma is used to define a Gaussian particle with global distortion, whereas, in light scattering computations involving ice crystals, surface roughness is locally defined (see the following two papers):

Macke, A., J. Mueller, and E. Raschke, 1996: Single scattering properties of atmospheric ice crystal, J. Atmos. Sci., 53, 2813–2825.

Yang, P., and K. N. Liou, 1998: Single-scattering properties of complex ice crystals in terrestrial atmosphere. Contr. Atmos. Phys., 71, 223–248.

Note, most ice crystals are faceted particles. Thus, the ke-sigma relation shown in Figure B1 should not be generalized to realistic ice crystals. Some further studies may be required to apply the parameter ke to the computation of ice crystal optical properties.

In order to show the atmospheric relevance of the Gaussian particle model, we calculated the area ratio α and the effective density ρ_e of the model particles shown in Fig. B1. These values are given in the revised version of Fig. B1. The values are well in agreement with the recent Cloud Particle Imager (CPI) observations of $0.6 < \alpha < 0.8$ for small (< 50 µm) ice particles in Arctic ice clouds (McFarquhar et al., 2013) and ρ_e=700 kgm^{-3} for small ice particles measured in mid-latitude cirrus clouds using the SID-2 instrument (Cotton et al., 2013). Therefore, our idealized optical model is consistent with the most recent microphysical observations and it is justified to use this model to get a first rough correlation between the complexity parameter k_e deduced from SID-3 and the geometrical particle complexity. We are aware of the fact that ice particles are in general faceted (despite frozen droplets for which the Gaussian sphere model might be more realistic (Nousiainen et al., 2011)). Therefore, it is our intention to test the SID-3 complexity analysis with more realistic optical models for hexagonal cirrus ice particles in the future.

Nousiainen, T., Lindqvist, H., McFarquhar, G. M., and Um, J., 2011: Small Irregular Ice Crystals in Tropical Cirrus. Journal of the Atmospheric Sciences, 68(11), 2614–2627. http://doi.org/10.1175/2011JAS3733.1

4) On page 3, "For a better assessment ... (Baran, 2009)": For the authors' information, a comprehensive review of ice cloud optical properties and radiative forcing has been recently published, where the effect of particle surface roughness is discussed from remote sensing and radiative forcing perspectives:

Yang, P., K. N. Liou, L. Bi, C. Liu, B. Q. Yi, and B. A. Baum, 2015: On the radiative properties of ice clouds: Light scattering, remote sensing, and radiation parameterization. Adv. Atmos. Sci., 32(1), 32–63, doi: 10.1007/s00376-014-0011-z

We agree that this review article is important when presenting and discussing the current knowledge of ice particle surface roughenss from remote sensing and radiative forcing perspectives. We have added a citation to this article to the Introduction section.

5) An asymmetry factor of 0.78 is questionable (see the abstract). The measurements do not provide the scattering functions in the forward and backscattering angles. The theoretical values in Fig. 7 are based on a combination of spheres and roughened hexagonal columns. The scattering maximum near 170 degrees may be an artifact. There may be other phase functions that can fit the measurements in the scattering region between 20-160 degrees, which may give quite different asymmetry factor values.

We agree with the reviewer that the determination of the asymmetry parameter from a comparison of the nephelometer measurements with a published model scattering function is not justified. Although this might be possible to some extent - either by extrapolating the missing forward scattered intensity based on the method presented by Gerber et al. (2000) or by using the iterative inversion method developed by Oshschepkov et al. (2000) and Jourdan et al. (2003) - the main conclusions from Fig. 7 as listed and discussed in Section 3.3 are still valid. We therefore believe that our results are of high relevance for the real atmosphere. However, we see that the reader might be misguided by giving the asymmetry parameter of the model scattering function in the discussion of Fig. 7 in Section 3.3, and we have revised this section as well as the Abstract and the Conclusions accordingly.

Gerber, H., Takano, Y., Garrett, T. J., & Hobbs, P. V., 2000: Nephelometer Measurements of the Asymmetry Parameter, Volume Extinction Coefficient, and Backscatter Ratio in Arctic Clouds. Journal of the Atmospheric Sciences, 57(18), 3021–3034.

Oshchepkov, S., Isaka, H., Gayet, J.-F., Sinyuk, A., Auriol, F., & Havemann, S., 2000:

Microphysical properties of mixed-phase and ice clouds retrieved from in situ and airborne "Polar Nephelometer" measurements. Geophysical Research Letters, 27(2), 203–212.

Jourdan, O., Oshchepkov, S., & Gayet, J.-F., 2003: Statistical analysis of cloud light scattering and microphysical properties obtained from airborne measurements. Journal of Geophysical Research, 108(D5), 4155 (1–6).

We thank the anonymous reviewer #2 for the helpful comments. These comments helped to substantially improve the manuscript. Below we give detailed answers to the individual reviewer comments in blue.

This paper provides new insights into the relationship between atmospheric state variables and ice crystal complexity through the novel and original use of cloud chamber experiments. Previous cirrus in situ-based work has failed to find such relationships because real atmospheric ice particles undergo different cycles of subsaturation and supersaturation, resulting in weak evidence. This laboratory-based paper reports results based on well controlled experiments of single cycles of subsaturation and supersaturation, with respect to ice, measured over some interval of time. As a result of this more systematic approach, they find correlations between ice crystal complexity and atmospheric state variables. At the same time, as these controlled experiments SID-3 two-dimensional light scattering patterns are obtained, and these were used to estimate surface roughness or ice crystal complexity, which could then be related to supersaturation w.r.t ice. They report a positive correlation between ice crystal complexity and atmospheric state variables. They also make good use of an electromagnetic method by applying it to a distortion of the sphere to derive the speckled 2D patterns measured by SID-3. By increasing the model distortion value they show that this too is related to their proxy for surface roughness, and hence atmospheric state variables. Moreover, a previously fitted phase function is applied to their laboratory results and from that they deduce an asymmetry parameter value of 0.78. A useful light scattering modelling result to come out of this paper is the experimental confirmation that once the ice particle is sufficiently randomised, the resulting measured light scattering pattern is invariant with respect to shape. Finally, they generalise their laboratory-based findings to the real atmosphere. This paper is an important step along the way to understand why atmospheric ice particles are observed to be generally complex. This paper should be published, but only after the following points have been considered and discussed.

1. There are numerous examples of typos, incomplete sentences, and incorrect words. Please could the authors more thoroughly proof read their paper before resubmitting a revised version?

We will thoroughly proof read the revised paper before submission.

2. The authors define ice crystal complexity as "...any kind of crystal distortions (surface roughness, polycrystals, aggregates, (stepped) hollowness).." and yet their measure of complexity is best related to surface roughness according to Lu et al. (2006). That paper does not state anything about the dependence of k_e on any of the other variables listed in their definition of ice crystal complexity. Therefore, are the authors saying that their SID-3 laboratory measurements are more related to surface roughness than the other variables listed? Given the size range listed, and their figure 5 caption, which shows no aggregates or polycrystals and states "...surface properties are masked by the Formvar replication method...". Given the above, it seems to this reader that their results are indeed more related to surface roughness and so for this paper their definition of ice crystal complexity is redundant? They have yet to show the dependence of the SID-3 light scattering patterns on all the other variables inclusive of surface roughness. This is an important point, as it is necessary to show whether surface roughness alone is sufficient to replicate the SID-3 measurements, even if the particles might also be hollow, polycrystalline, rosettes, plates or aggregate combinations of some or all of these shapes.

In the presented experiments, we have only single particles present, so, particle aggregation can be excluded from the list of complexity types that influence k_e. Polycrystallinity and hollowness, on the other hand, are clearly present in our ice particle populations (Fig. 5). As k_e is a measure of the degree of spatial randomization of the scattered light intensity, it is currently not possible to discriminate these complexity types from surface roughness without any further information. For example, the speckle patterns produced by fine-roughness mineral dust grains and highly complex ice analogue crystals are similar, as previously shown (Ulanowski et al., 2014). However, in the case of hollow columns there are indications of a specific triangular feature around the 22° halo spots of the scattering patterns (visible on the second pattern of row (b) in Fig. 1), which might be useful to discriminate this complexity type in future.

We have changed our complexity definition to “all surface distortions on a single ice particle (surface roughness on a variety of scales, polycrystallinity, and hollowness)”, and named it “small-scale complexity”. In this way, we think there is a clear differentiation to large-scale complexity that is induced by crystal aggregation and that can be easily observed by high resolution imaging (e.g. Schmitt and Heymsfield, 2014).

3. The discussion in the main text is related to k_e and not the parameter referred to as the “image texture feature energy” in the caption of Figure 1. What exactly is the latter? Since they use the former, perhaps the latter could be removed? If it is important how else is it used? Its quantitative use is not at all clear?

We agree with the reviewer that the “energy feature” does not add any further information and actually isn’t used for data interpretation in the manuscript. So, we omitted the energy feature from the image and caption of Figure 1.

4. In the introduction, page 6, line 5. The authors only discuss surface roughness with regard to the uncertainties in cirrus radiative effects in a climate model. There are of course a number of other important cirrus properties that contribute to this uncertainty apart from surface roughness. Surface roughness is important, but there are a number of other properties that must also be considered, and the uncertainties associated with these may have the greater impact on cirrus radiative effects. These are the amplitude and distribution of the small ice mode, the shape of the PSD, the distribution of shapes across the PSD, and the shape distribution as a function of distance from the cloud-top. The authors should cite the following papers that discuss all the above (there are of course others, but these are representative) and these are listed as follows:

(1) Mitchell, D. L., P. Rasch, D. Ivanova, G. McFarquhar, and T. Nousiainen (2008), Impact of small ice crystal assumptions on ice sedimentation rates in cirrus clouds and GCM simulations, Geophys. Res. Lett., 35, L09806, doi:10.1029/2008GL033552

(2) Anthony J. Baran, Peter Hill, Kalli Furtado, Paul Field, and James Manners, 2014: A Coupled Cloud Physics–Radiation Parameterization of the Bulk Optical Properties of Cirrus and Its Impact on the Met Office Unified Model Global Atmosphere 5.0 Configuration. J. Climate, 27, 7725–7752. doi: http://dx.doi.org/10.1175/JCLI-D-13-00700.1

(3) Yang, H., Dobbie, S., Herbert, R., Connolly, P., Gallagher, M., Ghosh, S., Al-Jumur, S. M. R. K. and Clayton, J. (2012), The effect of observed vertical structure, habits, and size distributions on the solar radiative properties and cloud evolution of cirrus clouds. Q.J.R. Meteorol. Soc., 138: 1221–1232. doi:10.1002/qj.973.

We agree with the reviewer and added the following sentence to page 5, 1st paragraph: “As already mentioned, the uncertainties in assessing the radiative effect by cirrus clouds are due to the uncertainties of many macrocscopic as well as microscopic cloud properties like IWC, the vertical structure of the ice particle size and shape distributions, the amplitude and distribution of the small ice mode, etc. (Mitchell et al, 2008; Yang et al., 2012; Baran et al., 2014).”. However, we would like to emphasize that although the prediction of cloud formation and evolution is important, the optical properties of the constituent ice particles eventually define the radiative effect of the cloud once it has been formed.

5. In the introduction, page 4, 3rd paragraph, line 4. Once again, in my opinion, there needs to be more of a balance in the choice of citations, as the citations chosen appeared after others had already shown some of their results. The discussion is essentially about the consistency of models using observations from across the spectrum and the evidence so far tends to show that

randomised models are better at simulating simultaneous multi-spectral, multi-angle observations. Other citations that ought to be included are listed as follows:

(1) Baran, A. J. and Francis, P. N. (2004), On the radiative properties of cirrus cloud at solar and thermal wavelengths: A test of model consistency using high-resolution airborne radiance measurements. Q.J.R. Meteorol. Soc., 130: 763–778. doi:10.1256/qj.03.151

(2) Baran, A. J., Havemann, S., Francis, P. N., and Watts, P. D. A consistent set of single-scattering properties for cirrus cloud: tests using radiance measurements from a dual-viewing multi-wavelength satellite-based instrument. Journal of Quantitative Spectroscopy and Radiative Transfer,79-80, 549-567, 2003

(3) Baran, A. J., Cotton, R., Furtado, K., Havemann, S., Labonnote, L.-C., Marenco, F., Smith, A. and Thelen, J.-C. (2014), A self-consistent scattering model for cirrus. II: The high and low frequencies. Q.J.R. Meteorol. Soc., 140: 1039–1057. doi:10.1002/qj.2193.

We agree with the reviewer and have added the suggested references accordingly.

6. In the introduction, page 4, line 12. Field et al. (2003) used mid-latitude SID-2 measurements to test the angular scattering properties of models, so this paper should also be cited. In Field et al. (2003), no evidence for halos was found.

Field, P. R., A. J. Baran, P. H. Kaye, E. Hirst, and R. Greenaway (2003), A test of cirrus ice crystal scattering phase functions, Geophys. Res. Lett., 30, 1752, doi:10.1029/2003GL017482, 14.

We added the following sentences to page 4: “Field et al. (2003) analyzed SID-2 single particle scattering patterns in order to draw conclusions on the scattering phase function of cirrus ice crystals. They found no evidence for 22° halos in their data set of mid-latitude cirrus.”

7. As stated in point 4 above, determining the small ice mode is important and the authors of this paper are aware of this problem. Unfortunately, in this paper, there are no comparisons of PSDs measured by the differing instruments. Please show examples of such comparisons. The speckle pattern reported in this paper could also be used to determine ice crystal size as shown by Ulanowski et al. (2012) [JQSRT 113, 2457-2464]. How does this method compare to independent measurements of small ice?

We agree that the small ice particle mode is important for the radiative properties of cirrus clouds and the measurement of this microphysical property is highly uncertain due to the different methods used by in-situ cloud probes. In the AIDA chamber, due to the experimental conditions, we know that (i) we only have ice particles smaller than 50 µm and (ii) this small ice particle mode is not biased by particle shattering. Therefore, such experiments are extremely useful in comparing in-situ cloud probes although this was not the primary focus of this work. To give the reader an impression of the potential we have in this respect, we added the result of the PHIPS-HALO image analysis to panel (c) of Fig. 2. In doing so, this panel now shows a comparison of two different particle sizing methods; the laser scattering method used in PPD-2K and SID-3 and the imaging method used in PHIPS-HALO. Although the evolution of the size distribution agrees very well, there is a systematic size difference between the two instruments.

8. An example of one of the limitations of this study scaled to the real atmosphere is the reported infrequent occurrence of hollow ice crystals. However, in situ observations by Schmitt and Heymsfield (2007) [Schmitt, C.G., and A.J. Heymsfield, 2007: On the occurrence of hollow bullet rosette- and column-shaped ice crystals in midlatitude cirrus. Journal of the Atmospheric Sciences, 64, 4514-4519, DOI: 10.1175/2007JAS2317.1] show that hollow ice crystals can frequently occur at cirrus forming temperatures. Moreover, the cloud chamber study of Smith et al. (2015) [Smith , H R , Connolly , P J , Baran , A J , Hesse , E , Smedley , A R D & Webb , A R 2015, Cloud

chamber laboratory investigations into scattering properties of hollow ice particles, Journal of Quantitative Spectroscopy and Radiative Transfer , vol 157 , pp. 106-118 ., 10.1016/j.jqsrt.2015.02.015] report that stepped hollow columns can reduce the asymmetry parameter, relative to other forms of cavity that are usually assumed, and these occurred frequently in their experiments at temperatures down to -30°C. Therefore, the geometric form of cavity assumed will affect the asymmetry parameter. The current studies are limited to a narrow size range and ppmv values, and so cannot be expected to cover the size range measured in the studies reported above. The authors should discuss in more detail the limitations of scaling their laboratory results to the real atmosphere.

It is possible that the reviewer might have misinterpreted our results. The term "occasional" is related to the observation of stepped hollowness that we classified as surface roughness type of complexity. The fact that stepped hollowness was infrequently observed in our experiments is rather due to the limitations in the used imaging methods - a high level of magnification is required to resolve stepped hollowness - then being a property of the particle ensemble. In fact, we observed hollowness quite frequently in the imaging data (replica and PHIPS) especially in the -50°C runs and for S_{ice} above 1.15 and it is likely that at least a part of this hollowness is stepped. Therefore, we think that our results are in accordance with the studies mentioned by the reviewer and are of relevance for the real atmosphere.

We will discuss our hollowness observations more clearly in the revised paper to avoid further misinterpretations.

9. Section 3, page 18, line 23. The authors report a relationship between ice crystal complexity and supersaturation. Recently reported satellite-based observations by Baran et al. (2015) [Baran, A. J., Furtado, K., Labonnote, L.-C., Havemann, S., Thelen, J.-C., and Marenco, F.: On the relationship between the scattering phase function of cirrus and the atmospheric state, Atmos. Chem. Phys., 15, 1105-1127, doi:10.5194/acp-15-1105-2015, 2015] tend to support this view. However, such a strong link could not be found statistically, due to there being too few cases. Nevertheless, in Figure 11 of that paper, it can be seen that pixels related to phase functions exhibiting ice bow features were more associated with low NWP model supersaturation values. Whilst pixels associated with phase functions exhibiting no features at backscattering angles were mostly associated with supersaturation values >>1. Note also, the range in asymmetry parameter values reported in that paper was between 0.82 and 0.79. A 5% difference in the asymmetry parameter is climatically important. This is why we need to understand the relationship between ice crystal complexity and the atmospheric state.

We agree with the reviewer that the mentioned satellite-based study supports one of our main findings from the laboratory, namely a correlation between ice crystal complexity and supersaturation. Therefore, we added a paragraph to Section 4, in which we discuss our laboratory results in the context of the study by Baran et al. (2015).

10. The question arises as to how such a relationship can be incorporated into climate models? This paper provides the first steps towards this eventual aim through Figures 4 and 6. However, there does need to be a comment about Figure 6. From this figure, it would seem that for mixing ratios >~5 ppmv complex particles can be assumed or roughened particles, and from Figure B2 this occurs at distortion values >~ 0.4, and Fig. B1 suggest that surface amplitude irregularities need to be significant. However, this value of 5 ppmv is very small within a climate model. Are the authors sure that this figure is correct? Or rather are the numerical values along the x-axis correct? The authors use ppmv, whereas in atmospheric models mixing ratio is usually in units of kg per kg and 5 ppmv translates to about ~10^{-6} kg per kg? In some atmospheric models, this value is taken as the threshold value for the existence of cloud. Therefore, the authors imply that in atmospheric models, the ice particles should always be rough as non-roughened ice particles cannot exist in such models. At least according to their threshold value or is there an error somewhere? This could be yet another limitation of this experiment to the real atmosphere? Please

comment. Moreover, why not on the x-axis just plot the results in kg per kg? As this unit is more directly related to atmospheric models whereas ppmv is more related to chemistry.

Here, we have to emphasize that in Fig. 6 we have plotted the median roughness parameter over the available condensable water vapor mixing ratio. The latter is not the absolute water vapor mixing ratio as it is usually calculated by numerical weather prediction models, but the mixing ratio of those molecules that are in excess with respect to the molecular number concentration at ice saturated conditions, i.e. the difference between the absolute mixing ratio and the mixing ratio at ice saturated conditions for the actual pressure and temperature in the chamber. Therefore, this value is inherently zero at ice saturated conditions. We introduced this quantity here because we wanted to compare the complexity results of the two sets of experiments performed at initial temperatures of -40°C and -50°C in Figure 6 without the superimposed ice saturation vs. temperature dependence that is inherent in Figure 4. We believe that this is explained in a clear and sufficient way in Section 3.1 of the manuscript.

The reviewer is correct, when pointing out that the study presented here is the first step to understand the formation of crystal complexity of atmospheric ice particles. However, further work is still needed to implement these results in climate models.

11. The experiments of substaturation and supersaturation are over a single cycle. What would happen to the ice particle complexity if several cycles were measured? In the real atmosphere, cirrus ice particles undergo a number of cycles, and this might completely change their level of complexity such as the formation of polycrystals, and these in turn, will change their scattering properties and g-values. Please comment and discuss.

As already mentioned in the description of step 5 of the growth and sublimation cycles (Sect. 2.2.2), several regrowth cycles can be performed within the same cloud provided that a significant ice particle number concentration is left in the chamber from the previous cycle. Actually, nine of the data points shown in Figs. 4 and 6 are from higher order regrowth cycles. Typically, these higher order cycles were performed at higher supersaturations then the previous cycles, just because the ice crystal concentration is decreasing with time and therefore higher supersaturation levels can be reached at later times. These data points nicely fit to the general trends given in Figs. 4 and 6, i.e. there are no indications that a possible formation of polycrystals with time has a significant influence to the results. However, there is one cycle where the second regrowth was performed at lower S_{ice} (1.04 vs. 1.18 as in the first cycle). This cycle indeed results in a slightly higher complexity parameter (k_e=4.49) of the ice crystals compared to first order regrowth experiments at similar S_{ice} ($k_e \approx 4.3$). In conclusion, the formation of polycrystals with time might result in a slight increase of the crystal complexity within the ice cloud, but this does not change the general results and conclusions of the study.

12. Figure B1. Please can the authors, for each assumed distortion value, provide the corresponding model area ratio and particle effective density? How well do these values compare to more recent observation of small ice area ratios and effective densities? More recent observations of these parameters can be found, respectively, in the following list of papers:

(1) Greg M. McFarquhar, Junshik Um, and Robert Jackson, 2013: Small Cloud Particle Shapes in Mixed-Phase Clouds. J. Appl. Meteor. Climatol., 52, 1277–1293 doi: http://dx.doi.org/10.1175/JAMC-D-12-0114.1

(2) Cotton, R. J., Field, P. R., Ulanowski, Z., Kaye, P. H., Hirst, E., Greenaway, R. S., Crawford, I., Crosier, J. and Dorsey, J. (2013), The effective density of small ice particles obtained from in situ aircraft observations of mid-latitude cirrus. Q.J.R. Meteorol. Soc., 139: 1923–1934. doi:10.1002/qj.2058.

Just because the assumed idealised model can be made to produce a speckled pattern does not mean that the model is consistent with the most recent observations of microphysics in terms of area ratio and mass. These parameters are also important to cirrus radiative transfer. Another idealised model, based on varying the Chebyshev model along the directions of theta and phi, which could also be considered by the authors is described here http://www.ncbi.nlm.nih.gov/pubmed/21716343. Does this model also produce speckled patterns? It would be interesting to see.

We have calculated the area ratio α and the effective density ρ_e of the model particles shown in Fig. B1. These values are given in the revised version of Fig. B1. These values are well in agreement with the more recent observations of $0.6 < \alpha < 0.8$ for small (< 50 μm) ice particles in Arctic ice clouds (McFarquhar et al., 2013) and ρ_e=700 kgm^{-3} for small ice particles in mid-latitude cirrus clouds (Cotton et al., 2013). Therefore, our idealized optical model is consistent with the most recent microphysical observations and it is justified to use this model to get a first rough correlation between the complexity parameter k_e deduced from SID-3 and the geometrical particle complexity. We are aware of the fact that ice particles are in general faceted (despite frozen droplets for which the Gaussian sphere model might be more realistic (Nousiainen et al., 2011)). Therefore, it is our intention to test the SID-3 complexity analysis with more realistic optical models for hexagonal cirrus ice particles in the future. Although it would be interesting, testing other optical models (like the suggested Chebyshev model) is beyond the scope of this paper.

Here, we would like to emphasize an important point in the interpretation of microphysical observations. As has been shown in a conference contribution by Ulanowski et al. (2004) http://vuh-la-risprt.herts.ac.uk/portal/services/downloadRegister/426101/101433.pdf (Figs. 5 and 6), the microphysical properties of small near-spherical ice crystals determined from CPI images (as used in the study by McFarquhar et al., 2013) do not necessarily give information on the small-scale crystal complexity. This means that also in recent microphysical observations, part of the crystal complexity is hidden due to resolution limitations of imaging cloud probes. It has been recently shown by Ulanowski et al. (2014) and Järvinen et al. (2016) that this hidden small-scale crystal complexity can dominate the light scattering properties of small, near-spherical ice particles.

13. A comment on Figure 7. Extrapolating the fit to this figure to deduce the asymmetry parameter is not convincing. Moreover, there are no observations at scattering angles <<~ 20° and at scattering angles >~158°. It is quite possible to arrive at an alternative extrapolation to the one provided (by simple examination by eye of the figure), and this would give a completely different value for the asymmetry parameter. Their extrapolation is not supported by measurements at lower or higher scattering angles as all scattering angles are required to deduce the asymmetry parameter. Unfortunately, from this figure, it is not possible to come to a definite conclusion about a value for the asymmetry parameter. Let alone extrapolate it to the real atmosphere as the figure is related to their experiments having only undergone single cycles. Moreover, the phase function structure predicted by the assumed model at scattering angles greater than 160° is not supported by the most recent multi-angle global observations of cirrus. See, for example, the paper at this link http://www.atmos-chem-phys-discuss.net/15/31665/2015/acpd-15-31665-2015.html. In particular, note that Figure 2a in the above paper shows that the PDF of sampled direction peaks at scattering angles at around 160°, and it is still significant at 170°. Figure 7, in the same paper, shows that models exhibiting significant phase function structure in the backscattering direction near to 180° do not satisfy the observations. The model of the phase function shown in Figure 7 cannot be extrapolated to the real atmosphere.

However, having said that, it is still important that in-situ probes not only measure the scattered intensity at forward scattering angles but also at backscattering angles near to 180°. The authors may wish to elaborate on this point in their paper. This point is also made by Baran et al. (2012). If measurements were available at near 180° backscattering angles, then the model shown in Figure 7 might have been rejected.

We agree with the reviewer that the determination of the asymmetry parameter from a comparison of the nephelometer measurements with a published model scattering function is not justified. Although this might be possible to some extent - either by extrapolating the missing forward scattered intensity based on the method presented by Gerber et al. (2000) or by using the iterative inversion method developed by Oshschepkov et al. (2000) and Jourdan et al. (2003) - the main conclusions from Fig. 7 as listed and discussed in Section 3.3 are still valid. Additionally, as already mentioned in the answer to the reviewer comment 11, part of the presented results are from multi-cycle growth experiments. We therefore believe that our results are of high relevance for the real atmosphere. However, we see that the reader might be misguided by giving the asymmetry parameter of the model scattering function in the discussion of Fig. 7 in Section 3.3, and we will revise this section as well as the Abstract and the Conclusions accordingly.

14. Why do the authors not show a time series of the SIMONE linear depolarization ratio covering the subsaturated and supersaturated cycles? This measurement seems to be briefly mentioned in their paper. Why not use this SIMONE measurement to test the model at backscattering angles near to 180° shown in Figure 7? Please comment and show.

It is not yet possible to use the SIMONE backscattering results to test the scattering model shown in Fig. 7 because this requires an absolute measurement of the scattered intensity which is not yet implemented. However, there are some interesting results of the SIMONE linear depolarization measurements with respect to ice particle complexity, which will be the subject of a forthcoming paper.

Given the above caveats about extrapolating the experimental results to the real atmosphere the discussion in section 4 needs to be substantially revised. Some of the references used in section 4 probably can no longer be used as support for their extrapolations simply because the cirrus microphysics references are highly likely to have suffered from the shattering of ice crystals on the inlets of the microphysical probes, and this problem is not discussed at all in the section and how it might have affected the results.

We agree and will revise section 4 accordingly.

We thank the anonymous reviewer #3 for the helpful comments. These comments helped to substantially improve the manuscript. Below we give detailed answers to the individual reviewer comments in blue.

Review of "Cloud chamber experiments on the origin of ice crystal complexity in cirrus clouds" by Schnaiter et al.

Recommendation: Accept after minor revision

This paper reports on the origin of ice crystal complexity and its influence on the angular light scattering properties of cirrus clouds based on cloud simulation experiments in the AIDA cloud chamber. Ice particles were grown by both homogeneous and heterogeneous nucleation, and subsequently grown and sublimation at super and sub-saturated conditions. Ice crystal complexity was subsequently deduced from light scattering patterns measured by the SID-3. The principle finding was that ice crystal complexity is dependent on the available water vapor, and that this complexity dominates the microphysics. As with observations from natural clouds, the measured scattering phase functions were featureless resulting in low asymmetry factors that differ from those of several idealized crystals that are used to make up common scattering libraries. I think the paper is appropriate for publication in ACP because it is the first effort that shows ice crystal complexity is correlated to the available water vapor, and shows that some of the featureless phase functions observed in nature can be replicated in a laboratory environment. Nevertheless, I think there are some aspects of the presentation that could be improved before the paper is accepted for publication. Many of these aspects have already been identified by the other reviewers of the paper, so I will restrict my comments to a few other aspects of the presentation and emphasize a couple of the points previously made.

The major comment I would make is that crystal complexity needs to be better defined or better described. There are many aspects of ice crystals that affect their complexity and how they affect radiation from their three-dimensional shapes and their complexity, to the small-scale surface roughness to variations in aspect ratios. I think crystal complexity goes much beyond surface roughness as is described in the introduction. I don't think this paper ever formally describes what exactly is meant by crystal complexity or gives any perspective about the importance of complexity in affecting radiative properties compared to other microphysical properties (e.g., aspect ratio, size, shape, etc.). I would recommend that such material be added to the introduction.

We agree with the reviewer that the definition of crystal complexity was not given in a nuanced way. Therefore, we have changed our complexity definition to "all surface distortions on a single ice particle (surface roughness on a variety of scales, polycrystallinity, and hollowness)", and named it "small-scale complexity". In this way, we think there is a clear differentiation to large-scale complexity that is induced by crystal aggregation and that can be easily observed by high resolution imaging (e.g. Schmitt and Heymsfield, 2014).

Related to the above point, details about the modeling work and the parameter ke are currently found in Appendix B. As this paper is about crystal complexity and ke is found to be the most robust feature parameter to characterize crystal complexity with the SID-3, I think this modeling work should not be relegated to an Appendix but rather should appear in the main body of the paper.

We were stimulated by the work of Lu et al. (2006) who concluded that k_e is the most robust measure of surface roughness. We applied this measure to the SID-3 scattering patterns in order to characterize ice crystal complexity. A clear description of k_e, what it means in terms of a physical roughness, and how it is determined from the SID-3 patterns is now presented in Section 2.1.2 of the revised manuscript. The robustness of this measure in case of single particle scattering patterns was tested with analogue ice particles as described in Appendix A. We added the result of this test to Section 2.1.2 of the revised manuscript.

A first rough correlation between the complexity parameter k_e and the geometrical particle complexity was found in the modeling study for deformed Gaussian spheres shown in Appendix B. We are aware of the fact that ice particles are in general faceted (despite frozen droplets for which the Gaussian sphere model might be more realistic (Nousiainen et al., 2011)). Therefore, it is our intention to test the SID-3 complexity analysis with more realistic optical models for hexagonal cirrus ice particles in the future. That is why we think that the presentation of this modeling study should stay in the Appendix rather than being moved to the main body of the manuscript.

Nousiainen, T., Lindqvist, H., McFarquhar, G. M., and Um, J., 2011: Small Irregular Ice Crystals in Tropical Cirrus. Journal of the Atmospheric Sciences, 68(11), 2614–2627. http://doi.org/10.1175/2011JAS3733.1

In terms of experimental procedure, the authors claim that a sublimation period was applied in order to remove the ice particle surface characteristics from the initial growth. How confident are they that they are removing all of these surface characteristics? It would seem that apart from a derived measurement of the scattering function, it would be very difficult to know how these surface characteristics are changing. In addition to the effects investigated by the authors, would any small scale imperfections in the ice nuclei have impacted the surface roughness, complexity, and scattering patterns as well?

As stated in step 4 of the procedure list given in Section 2.2.2, sublimating conditions are applied for a period long enough to see a significant change in the SID-3 scattering patterns. As we know from the characterization of the SID-3 complexity method (e.g. Fig. B1) the SID-3 scattering patterns are very sensitive to smallest changes of the surface properties. What we typically observe during the sublimation periods is a gradual change of the acquired scattering patterns to oval patterns as shown in the upper panel of Fig. 3. The appearance of oval patterns is not only restricted to pristine hexagonal columns as depicted in Fig. 3, but is also observed in case of complex speckled patterns. As a subsample of the acquired SID-3 scattering patterns are displayed online by the acquisition software, a visual monitoring of these patterns by the experimentalist during the sublimation period gives detailed information on how the particle surface properties are changing with time and if the sublimation period has applied long enough. This is now described more detailed in the revised version of the manuscript.

As mentioned in the Conclusions, we do not see a significant difference in the ice crystal complexity for the different heterogeneous ice nuclei. However, there are indications for a memory effect in the case of homogeneous nucleation in aqueous sulphuric acid particles. This first observation will be further investigated in upcoming chamber experiments.

Page 30513, line 16. Although the net radiative effect of a single cirrus cloud can be altered by this much, the global effect as a whole is much less. I think this point should be made more clear so as to avoid over stating the impact of complexity.

We extended the corresponding sentence by "..., though the global effect by cirrus clouds is much less."

I would recommend that a photo of the experimental setup be added to the manuscript.That gives more of a visual description of how the experiment was setup. Alternatively, a schematic of the experimental setup would suffice.

A schematic of the experimental setup can be found in Schnaiter et al. (2012). As there are no significant changes to this configuration, there is no need to show the same schematic again. However we added a reference to the Schnaiter et al. (2012) schematic to Section 2.2.1.

Page 30520, line 19: Is there any bias to the sample by restricting to images with a narrow mean brightness range between 10 and 25? Were any sensitivity tests done to determine the effect of broadening?

Broadening the brightness range has a small influence on the k_e analysis in a way that e.g. the rough particle fractions given in Tab. 1 would increase by a few absolute percent when lowering the lower limit from 10 to 5. The upper limit in brightness range has less an influence.

Page 30522, line 21: The speed of 10 m/s is substantially smaller than that which would be used in an aircraft flight campaign where many prior scattering phase functions were measured. Is there any impact of the flow velocity on your results?

We do not expect an influence due to the lower particle speed as the exposure time for the SID-3 image capture is not controlled by the residing time of the particle in the laser beam but is set to a fixed value of 2 µs.

Page 30523, last 2 paragraphs: Were any other cloud probes also used to make measurements during the cloud expansion runs? This might provide an interesting data set for comparison against the scattering functions.

In part of the experiments we also operated other cloud probes. Comparisons of the measurement results from those instruments with the light scattering measurements will be the subject of forthcoming papers.

Page 30524, line 5: Can you quote the uncertainty on water vapor measurements here since this is a critical parameter for interpreting the results?

The water vapor measurement in terms of the partial vapor pressure has an accuracy of better than ±3 % (Fahey et al., 2014). This value is given in the revised manuscript.

Page 30524, line 19: how much uncertainty was there in the saturation with respect to ice, and how repeatable were the measurements?

The accuracy of the saturation ratio with respect to ice is dominated by the accuracy of the water vapor measurement and, therefore, is in the range of ±0.03 (Wagner et al., 2010). This value is given in the revised manuscript.

Page 30527, line 2: Define all acronyms.

Acronyms are defined in the revised manuscript.

Apart from these minor points, I think this paper is acceptable for publication in ACP.

Manuscript prepared for Atmos. Chem. Phys. Discuss.
with version 2014/09/16 7.15 Copernicus papers of the LaTeX class copernicus.cls.
Date: 8 April 2016

Cloud chamber experiments on the origin of ice crystal complexity in cirrus clouds

M. Schnaiter[1], E. Järvinen[1], P. Vochezer[1], A. Abdelmonem[1], R. Wagner[1], O. Jourdan[2], G. Mioche[2], V. N. Shcherbakov[2], C. G. Schmitt[3], U. Tricoli[4], Z. Ulanowski[5], and A. J. Heymsfield[3]

[1]Institute of Meteorology and Climate Research – Atmospheric Aerosol Research, Karlsruhe Institute of Technology (KIT), Karlsruhe, Germany
[2]Laboratoire de Météorologie et Physique (LaMP), Clermont-Ferrand, France
[3]National Center for Atmospheric Research (NCAR), Boulder, Colorado, USA
[4]Institute of Environmental Physics, University of Heidelberg, Heidelberg, Germany
[5]Centre for Atmospheric and Instrumentation Research, University of Hertfordshire, Hatfield, UK

Correspondence to: M. Schnaiter (martin.schnaiter@kit.edu)

Abstract

This study reports on the origin of small-scale ice crystal complexity and its influence on the angular light scattering properties of cirrus clouds. Cloud simulation experiments were conducted at the AIDA (Aerosol Interactions and Dynamics in the Atmosphere) cloud chamber of the Karlsruhe Institute of Technology (KIT). A new experimental procedure was applied to grow and sublimate ice particles at defined super- and subsaturated ice conditions and for temperatures in the $-40\,^{\circ}$C to $-60\,^{\circ}$C range. The experiments were performed for ice clouds generated via homogeneous and heterogeneous initial nucleation. ~~Ice~~ Small-scale ice crystal complexity was deduced from measurements of spatially resolved single particle light scattering patterns by the latest version of the Small Ice Detector (SID-3). It was found that a high ~~ice~~ crystal complexity is dominating the microphysics of the simulated clouds and the degree of this complexity is dependent on the available water vapour during the crystal growth. Indications were found that the small-scale crystal complexity is influenced by unfrozen H_2SO_4/H_2O residuals in the case of homogeneous initial ice nucleation. Angular light scattering functions of the simulated ice clouds were measured by the two currently available airborne polar nephelometers; the Polar Nephelometer (PN) probe of ~~LaMP~~ Laboratoire de Météorologie et Physique (LaMP) and the Particle Habit Imaging and Polar Scattering (PHIPS-HALO) probe of KIT. The measured scattering functions are featureless and flat in the side- and backward scattering directions~~resulting in low asymmetry parameters g around 0.78~~. It was found that these functions have a rather low sensitivity to the small-scale crystal complexity for ice clouds that were grown under typical atmospheric conditions. These results have implications for the microphysical properties of cirrus clouds and for the radiative transfer through these clouds.

1 Introduction

Cirrus clouds are situated in the cold upper troposphere at temperatures typically below $-35\,^{\circ}$C, and, therefore, they are completely composed of ice particles (Guignard et al., 2012; Baran et al., 2012). With their persistent coverage of about 30 % in the mid-latitudes and up to 70 % in the tropics, these clouds are an important component of the Earth's energy balance (Guignard et al., 2012). The underlying net radiative effect is expressed by the difference between a cooling effect due to the reflection of incoming shortwave solar radiation (albedo effect) and a warming effect by the absorption of outgoing longwave terrestrial radiation (greenhouse effect). Both effects depend on the macroscopic properties of the clouds, like the ice water content (IWC) or the cloud optical thickness τ, as well as the size, shape, and crystal complexity of the constituent ice particles (Zhang et al., 1999).

The mean global net radiative effect of cirrus clouds is highly uncertain, because their solar albedo cannot easily be quantified due to the unknown scattering properties of the complex-shaped ice particles. The crystal complexity can alter the local net radiative effect of a cirrus cloud (with otherwise fixed macroscopic parameters) from -40 to $+20\,\mathrm{W\,m^{-2}}$ (Zhang et al., 1999), though the global effect by cirrus clouds is much less. Airborne in situ measurements of the microphysical properties of cirrus clouds have revealed an increasing wealth of different sizes, shapes, and crystal complexity (see e.g. Baran, 2012 for an overview). This clearly emphasizes that more specific studies are necessary on the link between the ice particle microphysical complexity and the macroscopic cloud radiative properties.

For a better assessment of the cirrus radiative effects, single particle light scattering models for different ice particle shapes and degree of crystal complexity have been developed over the last two decades ~~(Baran, 2009)~~ (Baran, 2009; Yang et al. , 2015) . These calculations have been stimulated by the remote sensing community, which need realistic ice particle light scattering properties to improve their retrieval algorithms. The cirrus ice crystal model used in these algorithms has successively been extended in order to cover the increasing ice cloud remote sensing observations like spectral reflection, polarization and depolarization. With these new observations, there is now increasing evidence that highly complex ice particles (irregular particles or crystals with rough surfaces) are necessary to get a consistent interpretation of the combined satellite observations ~~(Baum et al., 2011; van Diedenhoven et al., 2013; Liu et al., 2014; Cole et al., 2014)~~ (Baran et al., 2003; Baran and Francis, 2004; Baum et al., 2011; van Diedenhoven et al., 2013; Baran et al., 2014; Liu et al., 2014; Cole et al., 2014). The angular scattering function of such ice particles is calculated to be featureless with a flat trend at backscattering angles, so that the ice features observed in the scattering function of pristine ice particles, i.e. the 22° and 46° halos as well as the ice-bow at backscattering angles, are smoothed out. ~~This results~~ Field et al. (2003) analysed SID-2 single particle scattering patterns in order to draw conclusions on the scattering phase function of cirrus ice crystals. They found no evidence for 22° halos in their data set of mid-latitude cirrus. The featureless and flat scattering functions result in relatively low asymmetry parameters, g, below 0.8 for these particles and in retrieved g values between 0.75 to 0.78 inferred from recent remote sensing polarization observations (van Diedenhoven et al., 2013; Cole et al., 2014).

In-situ measurements of the angular light scattering function in mid-latitude cirrus clouds (Gayet et al., 1998, 2004; Febvre et al., 2009) as well as Arctic mid-level ice (Lampert et al., 2009) and mixed-phase clouds (Jourdan et al., 2010) by the Polar Nephelometer (PN, Gayet et al., 1997) revealed a low asymmetry parameter in the range from 0.76 to 0.79, indicating ice particles with deeply roughened surfaces. Ulanowski et al. (2006) measured the angular light scattering function of smooth and roughened ice analogue crystals in the laboratory. They deduced very low asymmetry parameters of 0.63 for rough hexagonal rosette crystals, which differ significantly from the parameters around 0.8 recorded for smooth rosettes.

Over the last few years, an increasing number of studies have been published that apply the environmental electron microscopy technique to investigate the surface properties of growing and sublimating ice particles over a wide range of temperatures (Pfalzgraff et al., 2010; Neshyba et al., 2013; Ulanowski et al., 2014; Magee et al., 2014). The common observation of these studies is a prevalent mesoscopic roughness topography of the ice crystal surfaces on the scale of 1–20 µm. Neshyba et al. (2013) derived a roughness parametrization from their micrographs and applied a ray-tracing model to calculate the expected consequences for the angular light scattering function. They calculated a significant reduction of the asymmetry parameter of about 0.04 to 0.06 due to the derived surface roughness. Although these investigations indicate a prominent mesoscale surface texture of the ice crystals with the ice saturation ratio as an important driving factor, the relevance of these findings for real atmospheric ice particles are still under debate.

As already mentioned, the uncertainties in assessing the radiative effect by cirrus clouds are due to the uncertainties of many macrocscopic as well as microscopic cloud properties like IWC, the vertical structure of the ice particle size and shape distributions, the amplitude and distribution of the small ice mode, etc. (Mitchell et al., 2008; Yang et al., 2012; Baran et al., 2014a) . Yet, if ice crystal surface roughness is a prevalent feature of atmospheric ice particles, the reduced asymmetry parameters of these particles has significant consequences for the cloud radiative effect as it was recently shown in a climate modelling study by Yi et al. (2013). They used the National Center for Atmospheric Research Community Atmosphere Model (CAM, version 5.1) and calculated the global net radiative effects of clouds consisting of smooth and severely roughened ice particles. A global-averaged difference of $-1.46\,\mathrm{W\,m^{-2}}$ was calculated between the runs with smooth and roughened ice particles, indicating that ice particle surface roughness has the potential to force the energy balance in a similar magnitude as the greenhouse gases but opposite in sign. However, the underlying assumption that all atmospheric ice particles have a similar degree of crystal complexity and, therefore, a similar low asymmetry parameter is highly questionable.

In the present study, the development of crystal complexity during cirrus ice particle formation and growth was investigated in controlled experiments at the cloud simulation chamber AIDA (Aerosol Interactions and Dynamics in the Atmosphere). A new experimental procedure was applied to grow and sublimate ice particles at defined super- and subsaturated ice conditions and for temperatures in the $-40\,^{\circ}\mathrm{C}$ to $-60\,^{\circ}\mathrm{C}$ range. In these experiments the following questions were addressed:

i. ~~what~~ What is the role of the thermodynamic conditions prevailing during ice particle growth for the crystal complexity?

ii. ~~does~~ Does the ice nucleation type, i.e. heterogeneous or homogeneous, has an influence on the ice crystal complexity?

iii. ~~what~~ What is the impact of ice crystal complexity on the angular light scattering function and the asymmetry parameter g?

The crystal complexity was deduced from single particle measurements by the latest version of the Small Ice Detector (SID-3), which has been recently applied in an aircraft field study by Ulanowski et al. (2014).

The SID-3 method to deduce single particle complexity is described in Sect. 2.1 followed by an introduction to the AIDA cloud chamber instrumentation and the experimental procedure in Sect. 2.2. It was found that ice crystal complexity is frequently observed in the simulated ice clouds and the degree of this complexity is dependent on the available water vapour during the crystal growth. A parametrisation was developed to link the crystal complexity to the available water vapour. This parametrisation as well as the link between the angular light scattering properties and ice crystal complexity are presented in Sect. 3. The atmospheric relevance of the results is discussed in Sect. 4 and the final conclusions are drawn in Sect. 5.

2 Methods

2.1 Quantification of ice crystal complexity and surface roughness

2.1.1 Measurement of high-resolution angular light scattering patterns

~~To measure crystal~~ Crystal complexity of individual small ice particles ~~we used~~ is measured using the Small Ice Particle Detector Mk. 3 (SID-3). ~~Here, it has to emphasized that~~ To differentiate single crystal complexity, which is the subject of the present study, to the complexity that is induced by crystal aggregation, we henceforth use the term "~~crystal complexity"comprises any kind of crystal distortions~~ small-scale complexity", which is often referred to as surface roughness. While large-scale complexity or crystal aggregation can easily be observed by high resolution imaging (e.g. Schmitt and Heymsfield, 2014), the characterisation of small-scale complexity needs a different approach, like the detection of high resolution scattering patterns described here. Small-scale complexity, therefore, comprises all surface distortions on a single ice particle (surface roughness ~~, polycrystals, aggregates,~~ on a variety of scales, polycrystallinity, and (stepped) hollowness~~, etc.~~) that results in the formation of speckles in coherent light scattering. The analysis of these spatial fluctuations in the scattered intensity of individual particles is the fundamental method of measuring single particle complexity with SID-3 (Ulanowski et al., 2014).

SID-3 is the latest version of a suite of airborne single particle cloud probes that were developed by the University of Hertfordshire, UK. The derivation of ice particle complexity from SID-3 measurements is possible, since the basic concept of the SID instruments differ from other airborne single particle scattering probes. While these probes measure the total scattered light intensity in forward direction, the SID instruments additionally quantify the spatial distribution of the forward scattered light at different resolution levels. The first version of the instrument uses six azimuthally arranged detectors, and was primarily designed to discriminate between super-cooled water droplets and ice particles (Hirst et al., 2001). The second versions, named SID-2 and SID-2H, were designed to detect azimuthal light scattering patterns with 24 and 28 detectors, respectively (Cotton et al., 2010; Johnson et al., 2014). Finally, SID-3 uses an intensified charged coupled device camera (ICCD) to acquire two-dimensional (2-D) forward light scattering patterns with an angular resolution of better than 0.1°. Details of the instrument set up and data acquisition can be found in Ulanowski et al. (2014) and ~~?~~ Vochezer et al. (2016) . Here, we want to briefly highlight those features of SID-3 that are important for the ice crystal complexity measurements.

~~As already mentioned, SID-3 is the first in situ cloud probe that measures highly resolved 2-D light scattering patterns of individual particles that have passed~~ In the SID-3 probe individual particles pass a 532 nm, 30 mW laser beam. ~~These~~ From these particles, 2-D light scattering patterns are acquired using a 780×582 pixels ICCD (Photek Ltd, UK) with a maximum repetition rate of 30 Hz. Although images can be stored as 12 bit TIFF files, we set SID-3 to store the patterns as 8 bit grey scale JPEG files to be consistent with the laboratory and field studies by Ulanowski et al. (2014) and ~~?~~ Vochezer et al. (2016) . Image brightness can be adjusted by changing the intensifier gain of the ICCD. For the chamber experiments, we have chosen gains of 175 or 180 in order to get a maximum of analysable scattering patterns (neither underexposed nor saturated) for the particle size range from about 3 to 30 µm.

In the case of the SID-3 instrument, the (usable) polar angular range covered by the annulus-shaped main detector aperture is 7° to 23° relative to the forward scattering direction. Representative examples of 2-D scattering patterns of single small ice particles that were nucleated and grown in our cloud chamber experiments are given in Fig. 1. Note that for pristine hexagonal ice columns the scattering patterns (given in panels a and b of Fig. 1) clearly show the 22° halo refraction peaks on the intense diffraction arc that corresponds to the c axis of the crystals. In the case of roughened or distorted columnar ice crystals (as shown in panels c and d of Fig. 1), speckles emerge in the angular regions outside the diffraction arcs indicating a more diffuse spatial scattering behaviour of the corresponding crystals. A description of how the scattering patterns are analysed to infer a measure of the crystal complexity is given in Sect. 2.1.2. Details on the experimental procedures to grow ice crystals with different degrees of complexity are presented in Sect. 2.2.2.

In addition to the 2-D scattering patterns, the triggering system of SID-3 stores scattering intensity data of all particles that have passed the sensing area of the instrument, i.e. also for those particles that were detected while the ICCD was still busy with the image processing of a previous particle. The maximum acquisition rate for trigger intensity data is 11 kHz. This feature allows us to (i) calibrate the trigger detector by a set of scattering patterns from water droplets and (ii) generate statistically well-defined particle size distributions based on the trigger intensity measurements. In the case of SID-3, the trigger intensity measurements are performed under a relatively narrow solid angle around the 50° direction with respect to the forward direction.Therefore, the measurement is biased by the particle orientation in the case of aspherical ice particles. For this reason, the trigger intensity measurements from the Particle Phase Discriminator (PPD-2K), the laboratory version of SID-3, was used in the present study to determine the particle size distribution of the chamber ice clouds. PPD-2K measures the light scattering intensity of each individual particle over the annulus-shaped main detector aperture which is less biased by particle orientation. In addition, PPD-2K has a specifically designed inlet nozzle that focusses the sampled particles to the sensitive area of the instrument which results in better counting statistics compared to SID-3. Details on the PPD-2K and the size calibration procedure can also be found in ~~?~~ Vochezer et al. (2016) .

2.1.2 Scattering pattern analysis

For the analysis of the 2-D scattering patterns, a comprehensive image processing and analysis software was developed using the Vision Development Module of the LabView^{TM} (National Instruments Inc., USA) package. A detailed description of the main analysis steps per scattering pattern can be found in ~~?~~ Vochezer et al. (2016) . These steps comprise

- the computation of the polar integrated azimuthal intensity profile for droplet/ice discrimination
- a Mie fit procedure of the azimuthally integrated polar intensity profile in the case of spherical particles to determine the droplet diameter
- a discrete fast Fourier transformation of the polar intensity profile for the shape classification of ice particles
- a speckle pattern texture analysis to deduce ice crystal complexity.

While the first three steps are explained in detail in ~~?~~ Vochezer et al. (2016) , the final speckle pattern analysis step is described in the following.

The crystal complexity analysis relies on the grey-level co-occurrence matrix (GLCM) method described in Lu et al. (2006). This method was originally developed in the context of quality control of surface treatment processes, and Ulanowski et al. (2010) transferred it for the first time to the analysis of SID-3 ice crystal scattering patterns. The GLCM method was further applied in a first study on ice crystal complexity of simulated cirrus clouds generated in the AIDA cloud chamber (Schnaiter et al., 2011) and in the analysis of SID-3 data of atmospheric ice particles by Ulanowski et al. (2014).

The GLCM ~~describes~~ represents a frequency matrix describing how often pairs of grey-levels occur in ~~the~~ a texture image for pixels separated by a certain distance Δd and along a certain direction~~(Haralick et al., 1973)~~. In case of the 8-bit grey-level scattering patterns generated by SID-3, the GLCM has a size of 128×128 elements, where each element $p(i,j)$ represents a specific pair of gray-level values given by the two matrix indices i,j. The values of the individual elements give the total number of the corresponding gray-level pairs that were found when the algorithm is moving pixel-wise across the scattering pattern. Illustrations of this procedure can be found in Figs. 3 and 4 of Lu et al. (2006) . Speckle pattern texture features can then be extracted from the GLCM~~.~~, like the energy or uniformity feature E that represents the sum of the squared elements in the GLCM

$$E = \sum_{i=0}^{m-1} \sum_{j=0}^{m-1} p(i,j)^2. \quad (1)$$

Routinely, the five features contrast, correlation, energy, entropy, and homogeneity are computed (see Haralick et al., 1973 for details). In addition to these texture features, a “combined roughness measure” as defined by Ulanowski et al. (2014) as well as the normalized energy feature parameter k_e are computed by the image processing software. The former is a combination of E with measures of the image brightness distribution which (i) has a clear correlation with the subjective particle surface roughness and (ii) is less sensitive to image brightness variations. The latter was introduced by Lu et al. (2006). They ~~found that~~ investigated the correlation of the GLCM features to the physical roughness for laser scattering patterns ($\lambda = 0.66\,\mu\mathrm{m}$) from standard grinding specimens with average surface roughness profile parameters R_a in the range from 0.05 µm to 1.6 µm. The energy feature E was found to have the best correlation to the physical surface roughness. Moreover, Lu et al. (2006) investigated the robustness of E for variances in the configuration of the measurement, e.g. laser power stability, and suggested an exponential fit to the energy feature vs. pixel distance function $E(\Delta d)$ as the most robust roughness measure. The energy feature parameter k_e then represents the coefficient of this exponential fit to the combined $E(\Delta d)$ curves that were calculated from the GLCM for the four distinct directions 0°, 45°, 90°, and 135°. In the present analysis algorithm, k_e is deduced based on the energy feature curves that are calculated for the first three directions. Each of the three curves covers the Δd range from 1 to 31. So, a total number of $3 \times 30 = 90$ GLCM are calculated and analysed per scattering pattern.

According to Lu et al. (2006) , the energy feature parameter k_e has "... a good relationship with the surface roughness; is more robust to the variances of the setup configuration, the position, and the orientation of the surface to be measured; and is the best feature parameter to characterize the surface roughness". They plotted the dependence of k_e on the physical surface roughness profile parameter R_a and found that for the R_a value range from 0.1 µm to about 0.4 µm the k_e values increase from 4 to 5.8, respectively. Moreover, k_e started to saturate at a value around 6 for R_a values larger than the laser wavelength. The robustness of k_e for the SID-3 optical system and for variances in laser power was also investigated in ~~this~~ the present work by using analogue ice particles residing on glass plates as test objects (see Appendix A for details). The result of this test (given in Tab. A1) shows that k_e varies by less than 1% over a broad image brightness range. Further, Discrete Dipole Approximation (DDA) light scattering calculations of deformed spherical ice particles were conducted for different deformation degrees in order to determine a relationship between the k_e value and the particle surface modifications. Details of this modelling work can be found in Appendix B. In summary, these tests show that (i) k_e is the most robust feature parameter to characterise small-scale crystal complexity with SID-3 and (ii) there is a correlation between the optical feature k_e and the physical surface ~~distortions~~distortion in the range from 0.1 µm to about 1 µm when k_e starts to saturate. The analysis and interpretation of the SID-3 data therefore rely on k_e as the primary measure for small-scale ice crystal complexity.

For this work the above listed scattering pattern analysis steps were restricted to images within a narrow mean brightness (grey level) range between 10 and 25. In this way we could minimize remaining image brightness biases on the GLCM analysis results. For this brightness range the relative standard deviation in k_e is only 0.7 % and the fraction of saturated pixels per pattern is always below 1 % even for the brightest images (see Appendix A).

2.2 Cloud chamber simulation experiments

The ice crystal growth experiments were conducted in the aerosol and cloud simulation chamber AIDA (Aerosol Interactions and Dynamics in the Atmosphere) of the Karlsruhe Institute of Technology. AIDA can be operated as an expansion chamber to simulate the atmospheric conditions in ascending cloud parcels in the temperature range down to $-90\,^\circ\mathrm{C}$. The general experimental procedure applied in these cloud expansion experiments has been described in several publications (e.g., Möhler et al., 2005a; Wagner et al., 2006, 2015; Schnaiter et al., 2012). In the present study, the chamber was used to simulate ice clouds in the cirrus temperature regime. A novel experimental procedure was developed to modify the ~~the~~ ice crystal surface properties and their degree of ~~surface~~ small-scale complexity through growth and sublimation periods at defined super- and subsaturated ice conditions. This method is different from the standard expansion procedure (see e.g. Möhler et al., 2005a) and is therefore described in more detail in Sect. 2.2.2. In the following section, ~~first~~ the chamber instrumentation is introduced that was applied in the experiments.

2.2.1 Instrumentation

We used the same instrument configuration as in the study of Schnaiter et al. (2012) with additional airborne cloud particle probes; the Polar Nephelometer (PN, Gayet et al., 1997), the Particle Habit Imaging and Polar Scattering probe (PHIPS-HALO) as well as a Formvar replicator very similar to the one used in Miloshevich and Heymsfield (1997). A scheme of the basic experimental set-up is shown in Fig. 5 of Schnaiter et al. (2012) .

PHIPS-HALO is a novel airborne cloud probe that has been developed and certified for the operation on-board the new German research aircraft HALO (High Altitude and LOng Range). PHIPS-HALO is a combination of a stereoscopic imager and a polar nephelometer to acquire (i) micrographs of individual ice particles from two directions at an optical resolution of about 2.5 µm and (ii) the polar scattering function of the same particle in the angular range from 1° to 170°. Details on the basic instrument concept and measurement methods can be found in ~~(Schön et al., 2011; Abdelmonem et al., 2011)~~ Schön et al. (2011) and Abdelmonem et al. (2011) for the prototype versions and in Abdelmonem et al. (2016) for the airborne version of the instrument~~and in upcoming publications~~. The polar nephelometer (PN) is an approved airborne instrument that measures, depending on the particle concentration, the polar scattering function of single particles or particle ensembles in the angular range from 3.5 to 169° (Gayet et al., 1997; Crépel et al., 1997).

Ice particle replica were generated on 35 mm transparent plastic film strips that were precoated with polyvinyl formal (Formvar). Precoating was produced at room temperature by brushing one side of the plastic film with a solution of 5 % Formvar in chloroform which results in a Formvar coating of about 100 µm. For the operation at the AIDA chamber the replicator was modified by a solvent dispensing system composed of ~ 3 m teflon tubing and a syringe pump located outside the insulating housing of the chamber. In this way the softening of the Formvar coating by dispensing dichloromethane to the strip could be externally controlled. We used dichloromethane to soften the coating prior to the impaction of ice particles because of its low freezing point of -95.1 °C (Takahashi and Fukuta, 1988).

The airborne instruments PN, PHIPS-HALO, and SID-3 were located underneath the chamber within the temperature controlled environment of AIDA. There, the instruments were installed into specific vacuum sealed canisters in a strictly vertical orientation. These canisters have a 10 mm inner diameter stainless steel sampling tube that penetrates the chamber wall and projects into the chamber volume by about 0.2 m. Each sampling tube is equipped with a horn-shaped inlet to minimize sampling artefacts. Within the instrument canister, the sampling tube terminates about 10 mm in front of the sensing area of the instrument. Each canister is connected via a mass flow controller to the central vacuum system of the AIDA facility. By applying a mass flow of typically 50 standard liters per minute (standard $\mathrm{L\,min^{-1}}$) cloud particles from the chamber volume can be sampled, accelerated to a speed of about $10\,\mathrm{m\,s^{-1}}$ in the sampling tube and measured when exiting the tube close to the sensing area of the instrument. The ice particle replicator was installed in a similar canister as the other airborne instruments but was aspirated by only 20 standard $\mathrm{L\,min^{-1}}$ in order to get a reasonable separation of the ice particle replica on the strip.

The PPD-2K has a vacuum sealed detection cell, so there is no need for installing the instrument in a separate canister. The detection cell is equipped with a focusing particle nozzle that produces a confined particle beam with a cross section of $2.5\,\mathrm{mm}^2$. This cross section is small enough to completely fit into the flat rectangular laser beam cross section of the instrument. In this way, the forward scattering intensity of all sampled particles is detected and analysed in terms of the equivalent optical particle diameter. Further details on the instrument design and the calibration procedure can be found in ~~?~~ Vochezer et al. (2016) .

Three different aerosol types were used in the cloud simulation experiments to initiate the ~~the~~ ice formation: soot particles from a graphite spark generator (GFG 1000, PALAS) (Möhler et al., 2005b), Arizona Test Dust (ATD) particles that were re-dispersed by a rotating brush generator (RGB 1000, PALAS) in conjunction with impaction stages to size select the $< 2\,\mu\mathrm{m}$ particles (Möhler et al., 2006) as well as aqueous sulfuric acid particles generated in a home-built H_2SO_4/H_2O nucleation generator (Wagner et al., 2008).

Aerosol number concentrations prior to and during the cloud expansion runs were measured with a condensation particle counter (CPC3010, TSI). Several modifications have been applied to the CPC in order to ensure reliable operation during the cloud expansion runs, i.e. at differential pressures between the sampling line and the environment of more than 500 hPa (Seifert et al., 2004). The aerosol number size distribution was measured with a scanning mobility particle sizer (SMPS, TSI) and an aerodynamic particle sizer (APS, TSI) (Möhler et al., 2006).

The presence of cloud particles inside the chamber is monitored by the laser light scattering and depolarization instrument SIMONE (Schnaiter et al., 2012). SIMONE measures scattered light from particles residing in the center of the chamber from near-forward (2°) and near-backward (178°) directions. The backscattered light is analysed with respect to its polarization state which facilitates the derivation of the linear depolarization ratio δ_l. Although SIMONE is routinely used to detect phase-transitions in aerosol and cloud particle ensembles, it has recently also been used to investigate the microphysical properties of corona-producing ice clouds (Järvinen et al., 2014).

Water vapour measurements are conducted in two ways: in-situ measurements by using a tunable diode laser (TDL) spectrometer (Ebert et al., 2005) to measure the interstitial water vapour mass and an extractive measurement for measuring the total (interstitial plus condensed) water mass. For the latter, we used a fast chilled-mirror frost-point hygrometer (MBW, model 373) that is located outside the insulating housing of AIDA and that is connected via a heated stainless steel tube to the chamber volume. The accuracy of the TDL and MBW measurements is ±3%. Further details on the water vapour measurements at AIDA can be found in Wagner et al. (2010) and Fahey et al. (2014).

2.2.2 Growth and sublimation cycles

A novel experimental procedure for the AIDA cloud chamber was developed in order to grow and sublimate ice particles at defined super- and subsaturated ice conditions. This procedure consists of the following main steps that are applied to the pre-cooled chamber. In the present work the experiments were conducted at initial chamber temperatures of $-40\,°\mathrm{C}$ and $-50\,°\mathrm{C}$.

1. Preparation: The chamber volume was cleaned by evacuation and flushing cycles. Then water vapour was added in excess to the evacuated cold chamber so that a thin ice coating was formed on the inner chamber wall. This humidification step was followed by refilling the chamber with dry synthetic air until a slight overpressure of about 1 mbar was reached. Homogeneous temperature and humidity conditions throughout

the volume were ensured by operating the mixing ventilator of the chamber. After these preparation steps, a saturation ratio with respect to ice S_{ice} of about ~~0.95~~ 0.95 ± 0.03 and a background particle number concentration of $\sim 0.1\,\text{cm}^{-3}$ were typically measured.

2. Aerosol addition: aerosol particles were generated by the respective aerosol generator (Sect. 2.2.1) and the aerosol flow was directed to the AIDA chamber. The AIDA particle number concentration was continuously monitored and the aerosol addition was stopped after the desired concentration had been reached. The aerosol size distribution was measured after a homogenization period of several minutes.

3. Initial cloud activation: A chamber expansion run was started by opening the valve to the vacuum pump. The suction capacity of the pump was controlled and was typically set to a value of either 60 % or 80 % of the full capacity, which is $250\,\text{m}^3\,\text{h}^{-1}$. The start of the expansion marks the reference time of the experiment run and is given as time zero in Fig. 2. As a consequence of the decreasing pressure, the gas temperature decreases at nearly constant wall temperature (see panel a of Fig. 2). The continuous increase in this temperature difference results in an increase of S_{ice} from slightly subsaturated into supersaturated conditions (blue line in panel b of Fig. 2). At a specific threshold supersaturation, that is dependent on the used aerosol type, ice starts to form. In our experiments, ice forms either by heterogeneous deposition nucleation on soot or mineral dust, or by homogeneous freezing in the case of aqueous sulfuric acid. The ice formation onset is clearly marked by the strong increase in the SIMONE near-forward scattering signal (black line in panel d of Fig. 2). After ice particles have been formed they grow on the expense of excess water vapour in the still supersaturated environment. Eventually, the size of the ice crystals is above the lower detection limit of 7 µm of the PPD-2K instrument, so that they are counted (red line in panel d of Fig. 2) and sized (colour plot in panel c of Fig. 2). At the same time the PHIPS-HALO instrument started to image ice particles as indicated by the mean equivalent sphere diameter shown in panel c of Fig. 2. The constant offset between

the two diameters plotted in panel c is due to the fact that ice particles have a lower differential scattering cross section compared to liquid water droplets in the angular range of the PPD-2K and, therefore, their size is underestimated by a factor of about 1.7 (Cotton et al., 2010) . The increasing ice water content in the chamber is also nicely reflected by the increasing difference between the total water and interstitial water mass measurements (black and blue lines in panel b of Fig. 2). Ice crystal growth continues as long as the expansion is maintained, e.g. until 310 s after start of the expansion in the example given in Fig. 2.

4. Sublimation period: As the initial growth of the ice particles depends on the specific ice nucleation properties of the aerosol used, the growth conditions in terms of supersaturation cannot be controlled. Therefore, a subsequent sublimation period was applied in order to remove the ice particle surface characteristics from the initial growth. For this purpose, a flow of dry synthetic air ($\sim 40\,\mathrm{m^3\,h^{-1}}$) was fed into the chamber immediately after the expansion had been stopped; resulting in a compression of the chamber volume and, thus, in an increase of the gas temperature. Consequently, the ice saturation ratio S_{ice} changed from supersaturated to subsaturated conditions due to the addition of dry air and the gas temperature increase (panel b of Fig. 2). By controlling the compression air flow, a defined saturation ratio can be adjusted. In the experiment shown in Fig. 2, the saturation ratio was set to about 0.8. As soon as the compression was applied, the ice particles started to sublimate as indicated by the decrease in the ice particle size (panel c of Fig. 2). The ice particles were forced to sublimate for a period long enough to see a clear change of their shape and surface properties, but short enough not to completely sublimate them. A sufficient particle surface processing by sublimation is indicated by the observation of oval SID-3 scattering patterns as shown in Fig. 3. A subsample of the scattering patterns acquired by SID-3 are displayed online by the instrument data acquisition software. A visual monitoring of these patterns is performed during the sublimation period in order to decide when the sublimation can be stopped.

5. Regrowth period: After the ice particle processing by sublimation had been completed, the regrowth of the ice particles was started. For this purpose, the addition of compressing air was stopped followed by a controlled expansion of the chamber volume (e.g. at 580 s experiment time in Fig. 2). Since the basic idea of this experimental procedure was to control the ice particle grow speed, the regrowth should happen at a specific but nearly constant supersaturation (e.g. about 1.05 in case of the experiment shown in Fig. 2). For this purpose, the expansion was manually controlled by tuning the suction flow, while monitoring the saturation ratio measurement. Depending on the target supersaturation, suction flow tuning was applied either by using a mass flow controller (range up to $\sim 100\,\mathrm{m^3\,h^{-1}}$) or by changing the suction capacity of the pump. In this way, the regrowth of the ice particles was conducted at a nearly constant supersaturation over periods of at least 200 s (indicated by the shaded areas in Fig. 2). Several regrowth periods at different supersaturations can be performed within one ice cloud by repeating steps (4) and (5), provided that the ice particle number concentration, which is decreasing by sedimentation and sampling losses, is still above $\sim 5\,\mathrm{cm^{-3}}$.

3 Results

For the present work, a total of 45 sublimation and regrowth experiments have been selected from the AIDA ~~campaigns~~ campaign HALO06 (preflight test campaign for the HALO aircraft; 02/2011) ~~,~~ and the AIDA Rough ICE particle campaigns RICE01 (11/2012), RICE02 (05/2013), and RICE03 (12/2014).

As the water vapour mixing ratio is frequently measured inside cirrus ice clouds, the basic idea of the regrowth experiments was to study the dependence of the ice particle complexity on the ice saturation ratio during the growth of the crystals. Therefore, the start and end times for each regrowth period were manually determined by examining the time curve of S_{ice} (blue line in panel b of Fig. 2) and identifying those periods where S_{ice} showed a plateau (as indicated by the shaded areas in Fig. 2). The results of the single particle scattering pattern analysis were then statistically analysed for these regrowth periods. As already mentioned, only scattering patterns within a narrow mean brightness (grey level) range from 10 to 25 were considered as valid patterns in this statistical analysis. Periods that had less than 100 valid scattering patterns were excluded from the study. For the same time periods, S_{ice} was averaged to determine the mean ice saturation ratio, to which the ice crystals had been exposed ~~to~~ during their regrowth.

The result of this analysis is shown in Fig. 4. Experiments that were started at initial temperatures of $-40\,^{\circ}$C and $-50\,^{\circ}$C are given as black and grey symbols, respectively. Note that the one sigma error bars given for S_{ice} represent the variations that are due to the manual control of the pumping speed in order to keep a constant saturation ratio. The median complexity parameter $\widetilde{k}_{\text{e}}$ clearly increases with increasing supersaturation in the case of the $-50\,^{\circ}$C experiments, and this trend is even steeper for the experiments that were conducted at an initial temperature of $-40\,^{\circ}$C. As for a given supersaturation the available condensable water mass is increasing with increasing temperature, the ice particles will grow faster at warmer temperatures and, consequently, more defects in the crystal lattice are expected. Ice particle habits and growth rates were measured in the laboratory by Bailey and Hallett (2004) for ice particles grown on thin glass wires over a broad temperature range from $-20\,^{\circ}$C to $-70\,^{\circ}$C. They clearly observed faster growth rates with higher supersaturations and warmer temperatures. At $-50\,^{\circ}$C and for supersaturations of 20 % and 40 %, growth rates of about ~~0.035~~ 0.035 µm s^{-1} and 0.07 µm s^{-1} were respectively measured for columnar ice particles. These results are in good agreement with the results of our own growth rate measurements by analysing PHIPS-HALO images (see Appendix C). At $-40\,^{\circ}$C and for the same supersaturation range, Bailey and Hallett (2004) measured growth rates that were higher by a factor of at least two compared to the $-50\,^{\circ}$C results. The authors also report an increase in crystal complexity with increasing supersaturation, mainly represented by the development of hollowness and the formation of rosettes. At $-50\,^{\circ}$C these growth instabilities started to appear at an ice supersaturation around 20 % which is in good agreement with the ice crystal habits that were found on the replicator strips (Fig. 5). At $-40\,^{\circ}$C a significant crystal complexity was already observed at supersaturations around 10 %.

3.1 Correlation between $\widetilde{k}_{\mathrm{e}}$ and the condensable water vapour mixing ratio $\xi_{\mathrm{v}}^{\mathrm{acw}}$

The previously discussed results by Bailey and Hallett (2004) as well as our own results from the optical imaging of laboratory grown ice particles indicate that the available condensable water mass is the driving factor for the crystal growth rate and finally the crystal complexity. Although these studies do not give insight into the ice particle surface properties (except the ~~occasionally observed stepped~~ observed (stepped) hollowness, Fig. 5), it is reasonable to assume that a high ice particle growth rate also results in the formation of surface complexity, like surface roughness and stepped hollowness. Therefore, the ice saturation ratio plotted in Fig. 4 for the $-40\,^{\circ}\mathrm{C}$ and $-50\,^{\circ}\mathrm{C}$ experiments was converted into the available condensable water vapour mixing ratio $\xi_{\mathrm{v}}^{\mathrm{acw}}$ given on the x axis in Fig. 6. In this approach, $\xi_{\mathrm{v}}^{\mathrm{acw}}$ was calculated as the difference between the measured interstitial water vapour mixing ratio ξ_{v} and the saturated mixing ratio $\xi_{\mathrm{v}}^{\mathrm{s}}$ for the given pressure and temperature conditions inside AIDA. $\xi_{\mathrm{v}}^{\mathrm{s}}$ was thereby calculated based on the parametrization of the ice vapour pressure by Murphy and Koop (2005). $\xi_{\mathrm{v}}^{\mathrm{acw}}$ therefore represents the mixing ratio of excess water molecules that can deposit to the solid ice face. This way of representing the SID-3 crystal complexity data results in a combined correlation between $\widetilde{k}_{\mathrm{e}}$ and $\xi_{\mathrm{v}}^{\mathrm{acw}}$ for the $-40\,^{\circ}\mathrm{C}$ and $-50\,^{\circ}\mathrm{C}$ experiments. Figure 6 confirms the assumption that the ice crystal growth rate also controls the ~~ice particle surface~~ small-scale ice particle complexity. The correlation can be quantified by fitting a simple linear regression model to the data which gives a least square functional dependency of

$$\widetilde{k}_{\mathrm{e}} = 0.088 \times \xi_{\mathrm{v}}^{\mathrm{acw}} + 4.22 \tag{2}$$

with $\xi_{\mathrm{v}}^{\mathrm{acw}}$ given in ppmv.

Another conclusion that can be drawn from Figs. 4 and 6 is that the observed correlation does not depend on the type of the used aerosol or nucleation mode (homogeneous or heterogeneous) which means that the thermodynamic conditions during the ice particle (re)growth control the crystal complexity or surface roughness and not the type of ice nucleus. There is one exception however; the regrowth experiments conducted at an initial temperature of $-50\,^{\circ}$C and using homogeneous nucleation in aqueous sulfuric acid particles to initiate the ice cloud (grey triangles in Fig. 6). These experiments result in higher $\widetilde{k}_{\mathrm{e}}$ values compared to the corresponding experiments with heterogeneous initial ice formation on soot (circles) or dust (stars) as well as homogeneous initial nucleation at $-40\,^{\circ}$C (black triangles). This indicates a "memory" effect in the ice crystal complexity for homogeneous nucleation at colder temperatures. A possible explanation for this observation could be the formation of concentrated H_2SO_4/H_2O residuals on the ice crystal surface, which affects the regular crystal growth. Such a separation into solid ice and unfrozen residual solution was observed by calorimetric measurements on aqueous H_2SO_4 droplets in the cirrus temperature range $190\,\mathrm{K} < T < 230\,\mathrm{K}$ (Bogdan et al., 2006; Bogdan, 2006). Although emphasized by the authors, the formation of a complete H_2SO_4/H_2O coating of the crystal surface was not unambiguously proven by these studies. However, the formation of such coatings can have significant consequences for the ice particle growth rate and the persistence of ice supersaturations in cirrus clouds (Bogdan and Molina, 2009) . Further studies with homogeneously nucleated ice particles are necessary to investigate the impact of unfrozen H_2SO_4/H_2O residuals on the ice crystal complexity.

3.2 Discussion of specific ice particle fractions

Table 1 gives examples of the SID-3 pattern analysis results for the regrowth experiments labelled in blue and red in Figs. 4 and 6. The fraction of rough particles is thereby calculated by setting a threshold value $k_{\mathrm{e}}^{\mathrm{thr}}$ of 4.6 and classifying all particles below this threshold as smooth (examples given in panels a and b of Fig. 1) and all particles equal and above as rough (examples given in panels c and d of Fig. 1). The fraction of columnar ice particles is calculated from a fast Fourier transformation of the polar integrated azimuthal intensity profile of the patterns according to the description given in ~~?~~ Vochezer et al. (2016) . While the fractions of rough particles and rough columns are clearly correlated with S_{ice} and $\xi_{\mathrm{v}}^{\mathrm{acw}}$, the fraction of columns stays rather constant at a value around 0.6 up to ice saturation ratios of about 1.15 followed by a significant decrease for higher supersaturations. This observation can be explained by the formation of hollow columns and rosettes at an onset saturation ratio between 1.15 and 1.2 which results in a distorted or changed symmetry in the corresponding light scattering patterns. Another result from Table 1 is the behaviour of the fraction of those crystals that have indications of a 22° halo in the scattering pattern. This fraction is deduced by a visual inspection of each individual valid scattering pattern for intensity spots around 22° that are clearly contrasted from surrounding pixels. Interestingly, this particle fraction is not depending on S_{ice} or $\xi_{\text{v}}^{\text{acw}}$ but is, except experiment 42 from RICE03, rather constant within the narrow range between 30 % and 40 %. For the interpretation of this result one has to keep in mind that the pixels in the 22° halo spot are always saturated due to the limited dynamic range of the ICCD camera of 8 bit. Therefore, the true intensity in the halo spot is unknown and, thus, it cannot be concluded from the fraction of halo particles whether and how strong a 22° halo would appear in the ice cloud. Even if it is unlikely that an ice cloud with roughened ice crystals would show a halo feature, it has to be kept in mind that there is always a significant fraction of the (small) hexagonal ice columns that show the 22° halo feature in the SID-3 scattering patterns also for those experiments with a very high crystal complexity.

3.3 Angular light scattering functions

For the three experiments from RICE03 labelled in red in Figs. 4 and 6 and listed in Table 1, polar scattering functions were measured by the polar nephelometers PN and PHIPS-HALO and are plotted in Fig. 7. The individual scattering functions given in Fig. 7 are mean values of all valid particle scattering functions measured during the regrowth periods. A valid particle scattering function has (i) an intensity above the background level for each individual angular channel and (ii) has no saturated channels. Scattering functions that do not fulfil these criteria were removed from the analysis. A background intensity is deduced for each individual channel and is subtracted from the valid particle scattering functions before averaging. In the case of the PHIPS-HALO instrument, channel crosstalk and sensitivity characteristics are taken into consideration by applying a correction matrix to the mean scattering function. See Jourdan et al. (2003) for a description of the channel correction in the case of the PN instrument. After this, the resulting mean particle scattering function is normalised so that its integral over the instrumental angular range equals 1.

Although there are systematic deviations in the normalized scattering functions deduced from the PN and PHIPS-HALO measurements, both instruments agree in the following observations:

i. ~~the~~ The measured scattering functions show only minor changes from experiment to experiment.

ii. ~~the~~ The scattering functions are rather flat and featureless with no clear indications of a 22° or 46° halo.

iii. ~~there~~ There are some indications of a slight ice bow-like feature in the 130° to 150° angular range.

Observations (i) and (ii) can be interpreted as the result of crystal complexity that randomizes spatial light scattering to a sufficient degree so that shape-dependent features, like halo features, are removed from the polar scattering function resulting in a flat function with no significant variations for the different experiments. Interestingly, the polar scattering function is rather insensitive over a range of ice particle growth conditions where the SID-3 method still sees significant differences in the small-scale complexity parameter $\widetilde{k}_{\mathrm{e}}$ (cf. Fig. 6). Although the particle scattering functions for very low $\widetilde{k}_{\mathrm{e}}$ values have not been measured, these results might indicate that after a certain crystal complexity is induced, the angular light scattering function is insensitive to further increases in this complexity. The corresponding threshold in terms of S_{ice} is quite low and around 1.1 for the ice clouds grown in the $-50\,^{\circ}\mathrm{C}$ temperature range. In terms of the temperature-independent condensable water vapour mixing ratio $\xi_{\mathrm{v}}^{\mathrm{acw}}$, this threshold is about 4.3 ppmv. However, further analyses of the scattering functions in the different phases of the experiment runs are necessary to come to a final conclusion on the sensitivity of the light scattering functions to the small-scale ice particle complexity.

Observation (iii) indicates a minor influence from regular or near-spherical ice crystals on the angular light scattering function of the ice clouds (Baran et al., 2012). A similar featureless scattering function with a slight indication of an ice bow-like feature was measured by the PN in a case study of a mid-level Arctic ice cloud (Lampert et al., 2009). A particle mixture composed of deeply roughened hexagonal columns and smooth ice spheres was necessary to represent this observation. The corresponding angular scattering function of this particle model has an asymmetry parameter g of 0.78 and is plotted as solid line in Fig. 7. A very good agreement between the modelled and measured scattering functions is found, which is astonishing given that the modelled function is retrieved for an Arctic mid-level (not cirrus) cloud at a mean temperature of $-24.3\,°C$. ~~This is a first indication~~ Here, it is important to note that the measurements do not cover the forward and backward angular ranges and, therefore, also other scattering function models with different asymmetry parameters likely can fit the measurements. Further modelling work is necessary that uses the measured particle size distribution in conjunction with the shape information from the PPD-2K, SID-3 and PHIPS-HALO measurements to constrain the ice particle microphysical scheme in the iterative inversion method that was used in Lampert et al. (2009) and detailed in Oshchepkov et al. (2000) and Jourdan et al. (2003) . Only such an inversion analysis would result in a more reliable model scattering function and asymmetry parameter.

However, while keeping in mind these restrictions, the good agreement of the scattering functions measured for laboratory generated ice clouds in the $-50\,°C$ temperature range with a scattering function retrieved for an Arctic mid-level cloud indicates that the above discussed complexity threshold for a rather insensitive ~~mean particle~~ scattering function might be of general nature and also valid for natural ice clouds. In conjunction with the main finding of our study, namely a fast developing ice particle complexity with supersaturation conditions, this indicates some important consequences for the light scattering properties of atmospheric ice particles that will be discussed in the following section.

4 Atmospheric implications

In the present study the ice supersaturation with temperature, i.e. the available condensable water vapour $\xi_{\text{v}}^{\text{acw}}$, was identified as the main driving factor for the formation of small-scale ice crystal complexity. This factor has a low threshold value of 4.3 ppmv for the growth of ice particles with a sufficient degree of crystal complexity. A strong randomization of the light scattering is the consequence of this complexity resulting in a featureless cloud angular scattering function ~~with a stable asymmetry parameter g~~ that is insensitive to further changes in the growth conditions. So, the question is how frequent such threshold conditions can be found in cirrus clouds in order to draw conclusions on the role of ice crystal complexity for the short-wave radiative properties of these clouds.

In a study by Krämer et al. (2009) in-situ water vapour data from Arctic, mid-latitude, and tropical cirrus were analysed and discussed in terms of the frequency of supersaturated conditions inside cirrus clouds. ~~They~~ The authors found frequency distributions of the ice saturation ratio S_{ice} that are symmetrically distributed around a peak value close to 1 for the $200 < T < 240$ K temperature range. Although high supersaturations up to the homogeneous freezing level were measured, information of the growth history can hardly be deduced from these data as the supersaturation quickly relaxes after a sufficient amount of ice particles have been nucleated. However, by applying a simple box model and assuming homogeneous nucleation, their modeled ice number concentrations agree well with the measured concentrations for reasonable updraft speeds indicating that the formation and growth pathway of the young cirrus particles could indeed started from high supersaturations.

In the Interhemispheric differences in cirrus properties from anthropogenic emissions (INCA) experiment, ice saturation ratio dependent cloud present fractions were deduced from in-situ particle measurements in northern and southern mid-latitude cirrus (Ström et al., 2003). Cirrus ice particle formation onsets were estimated by the interpretation of local minima in these fractions to be a consequence of the reduced detection efficiency of the cloud particle instruments in case of recently nucleated cirrus particles. Following this interpretation, the cirrus clouds were preferentially formed in the S_{ice} range between 1.4 to 1.55 and slightly below 1.3 for the ~~southern~~ Southern and Northern Hemisphere, respectively. It was suggested that this difference in the freezing thresholds is an effect of the different pollution levels in both hemispheres resulting in homogeneous ice nucleation as the dominant freezing mechanism in the relatively clean Southern Hemisphere and heterogeneous nucleation in the more polluted Northern Hemisphere (Haag et al., 2003). By taking into consideration that the frequency distribution of measured in-cloud temperatures during INCA was between -30 to $-60\,^{\circ}\mathrm{C}$ with a maximum at about $-50\,^{\circ}\mathrm{C}$ (Gayet et al., 2004), the ice particles nucleated and grew in an ice supersaturated environment that forces significant crystal complexity according to the chamber results shown in Fig. 4. In conjunction with the discussion of the light scattering data given in Sect. 3, it can be expected that the cirrus clouds probed during INCA should have angular scattering functions with (i) no indications of a 22° halo, and (ii) an asymmetry parameter g with only little variations in hemispheric as well as interhemispheric comparisons. Both expectations were indeed confirmed by in-situ PN measurements during INCA by Gayet et al. (2004). Based on a statistical analysis of angular scattering functions measured in the ~~northern and Southern Hemispheres~~ Northern and Southern Hemisphere a very stable asymmetry parameter was deduced ranging from 0.76 to 0.78 with almost no differences in the mean values for the ~~northern~~ Northern (0.767) and ~~southern~~ Southern (0.770) ~~hemisphere~~Hemisphere. Only about 3 % of all measured scattering functions showed a 22° halo feature, also with no significant differences between the northern and southern measurements. It was concluded that the angular particle scattering properties give no indications on privileged ice nucleation mechanisms in the two hemispheres, although it was indicated from the freezing onset analysis. ~~This is~~ Here it is important to note that even though it was ruled out by the authors, the results might be partially affected by ice particle shattering on the probe tips and inlets.

In a case study of a semi-transparent mid-latitude cirrus, Baran et al. (2015) analysed angular-dependent radiometric measurements from the PARASOL satellite in order to link the shape of the back-hemispheric angular scattering function to the relative humidity (RH_i) field predicted by a numerical weather model. Even though their data set was not statistically sufficient to find a strong correlation, the authors observed the tendency that cloud regions exhibiting an ice bow feature were more associated with low RH_i values, while regions with no features in the backscattering angular scattering function were associated to RH_i values larger than about 115%.

Both of the above observations are in accordance with the findings of the present paper where also no significant differences in the angular light scattering properties could be identified for growth conditions above about $S_i = 1.1$, although significant differences in the complexity parameter $\widetilde{k}_\mathrm{e}$ were deduced. The cirrus clouds probed during the INCA experiments ~~therefore~~ and observed in the Baran et al. (2015) case study, therefore, probably have formed in ice supersaturated conditions that were high enough to produce significant crystal complexity, irrespective of the ice nucleation mechanism. In addition to the SID-3 laboratory results, there are indications from airborne SID-3 measurements that the GLCM speckle analysis method might be sensitive to the nucleation mechanism (homogeneous or heterogeneous) in ice clouds composed of complex ice particles (Ulanowski et al., 2014).

5 Conclusions

In this paper the origin of ice crystal surface complexity and its consequences for the angular light scattering properties of cirrus clouds were investigated in specific cloud chamber experiments performed in the $-40\,^\circ\mathrm{C}$ to $-60\,^\circ\mathrm{C}$ temperature range. The particle surface complexity was deduced from highly-resolved angular light scattering patterns of single ice particles measured by the latest version of the Small Ice Detector (SID-3). Similar to the previous work by Ulanowski et al. (2014), a speckle texture analysis was developed based on the grey-level co-occurrence matrix (GLCM) as part of the SID-3 scattering pattern analysis package ~~(?)~~ (Vochezer et al., 2016) . It was found that the normalized energy feature parameter k_e of the GLCM is the most robust measure of crystal surface complexity. The angular light scattering function of the laboratory generated ice clouds was measured by the two currently available airborne polar nephelometers PN and PHIPS-HALO.

A new experimental procedure was applied at the AIDA cloud chamber to regrow ice particles at defined ice saturation levels after the crystal surface properties from the initial nucleation and growth phases have been removed in a sublimation period. The nucleation of ice particles was initiated by using three different aerosol types; soot particles and mineral dust for heterogeneous ice nucleation as well as sulphuric acid particles for homogeneous nucleation. For 45 stable regrowth periods, the median crystal complexity parameter $\widetilde{k}_\mathrm{e}$ was deduced from the individual SID-3 scattering patterns. Averaged angular light scattering functions were deduced from the polar nephelometers for three regrowth periods.

From the experimental results the following main conclusions can be drawn:

- ~~there~~ There is a clear correlation between the ~~crystal surface~~ small-scale crystal complexity deduced from the SID-3 measurements and the volume mixing ratio of available condensable water vapour $\xi_\mathrm{v}^\mathrm{acw}$. The correlation could be fitted by a simple linear functional dependence given in Eq. (2).

- ~~the particle surface~~ The small-scale particle complexity that develops during the crystal (re)growth is not influenced by the type of heterogeneous ice nucleus inside the crystal. However, there are indications for a memory effect in the case of homogeneous nucleation in aqueous sulphuric acid particles.

- ~~there~~ There are no significant differences in the measured angular light scattering functions of ice clouds that were regrown at $\xi_\mathrm{v}^\mathrm{acw} \geqslant 4$ although significant differences in $\widetilde{k}_\mathrm{e}$ were deduced from the SID-3 data. This indicates threshold conditions for the ~~particle surface~~ small-scale particle complexity leading to an insensitive cloud scattering phase function. The measured functions are featureless and flat in the side- and backward scattering directions~~resulting in a low asymmetry parameter g~~.

These results have significant implications for the radiative transfer through cirrus clouds as water vapour measurements indicate that the growth of cirrus ice particles starts at saturation ratios that are usually above the threshold conditions for the formation of surface complexity. Furthermore, ice particles with a high degree of ~~surface~~ small-scale complexity can be expected if the crystals were homogeneously nucleated because (i) the growth starts at high supersaturations and (ii) there are indications that concentrated H_2SO_4/H_2O residuals on the ice crystal surface affects further crystal growth. A prevailing ice crystal complexity in cirrus clouds would result in a low asymmetry parameter g and, consequently, in a stronger solar albedo effect. The presented chamber results indicate that for typical growth condition rather low variations in g are expected. However, combined in-situ measurements with SID-3 and PHIPS-HALO (or PN) in cirrus clouds that were formed under different thermodynamic conditions are necessary to prove these conclusions. Such data is available from the HALO aircraft campaigns Midlatitude Cirrus (ML-CIRRUS) and Aerosol, Cloud, Precipitation, and Radiation Interactions and Dynamics of Convective Cloud Systems (ACRIDICON-CHUVA). The results of these measurements will be the subject of forthcoming publications.

Appendix A: Characterisation of the normalized energy feature parameter k_e

~~According to Lu et al. (2006) , k_e represents the coefficient of an exponential fit to the normalized energy feature vs. pixel distance curves that were calculated for the four distinct directions 0, 45, 90, and 135throughout the grey-level image. In the present analysis algorithm, k_e is deduced based on the normalized energy feature curves that are calculated for the first three directions. Each of the three curves covers the pixel distance range 1 to 31. So, a total number of $3 \times 30 = 90$ are calculated and analysed per scattering pattern. See Figs.3 and 4 of Lu et al. (2006) for an illustration of how the grey-level co-occurrence matrix (GLCM) is calculated for different directions and pixel distances.~~

The conclusion given by Lu et al. (2006) that k_e is the most robust GLCM feature to quantify surface roughness was checked for the SID-3 set-up by the following procedure. An analogue ice particle aggregate with severely roughened surfaces was placed on a thin polycarbonate window with anti-reflective coating. See Krasinski et al. (2007) for a description on how these ice analogue particles can be produced in the laboratory. After a visual inspection of the analogue aggregate under the optical microscope (left image of Fig. A1), the sample particle was moved into the sensitive area of SID-3 and was fixed at this position. While the instrument was forced to continuously trigger, the laser power was varied from a few mW to its maximum power of 100 mW. In this way a series of SID-3 patterns was acquired for the same particle at the same orientation but for different laser intensities (see right image of Fig. A1 for an example). The latter variation results in images with different brightnesses. In a final step, the GLCM features k_e, energy, and combined roughness were statistically analysed for different grey-level ranges. The result of this analysis is given in Table A1. The test clearly shows that k_e is the most robust GLCM feature also in the case of quantifying ice crystal complexity with SID-3.

Appendix B: Modelling SID-3 scattering patterns of deformed particles

The problem of electromagnetic scattering is here treated through the DDA approach. We make use of the GDT-matrix code (Tricoli et al., 2015) developed to simulate the SID-3-like forward scattering pattern (the electromagnetic field is calculated in an annulus between 5 and 25° in the forward direction). In order to increase the upper bound of the size parameter that can be modeled, we use the publicly available code ADDA (Yurkin and Hoekstra, 2012) to calculate iteratively the inverse of the interaction matrix. The convergence is checked through comparisons of the phase functions obtained with ADDA and with Mie theory for the equivalent sphere. We find that for a refractive index of $m = 1.32$, it is possible to stabilize the iterative solver in ADDA using at least 1.5 millions of dipoles (i.e. at least 10 dipoles per wavelength). In this way we are able to simulate ice particles up to a size parameter of $x = 50$ (corresponding to a particle of equivalent radius of about 4 µm). Then, exploiting the equivalence of the transition matrix with the inverse of the interaction matrix, we import this matrix into the GDT-matrix code in order to reproduce the output format required for the SID-3 analysis algorithm. In fact, the square modulus of the electric field is calculated for the given forward scattering annulus and it is then plotted on a plane of 780×582 pixels. The simulated wavelength corresponds to the SID-3 laser beam i.e., 532 nm. In order to be able to apply the GLCM method, the output intensity plot is saved as 8 bit grey scale JPEG files. The mean intensity of the generated JPEG pictures is then rescaled to 20 (in order to be comparable with the brightness range restrictions used in the analysis as described in Sect. 2.1.2). We apply this method to deformed spherical particles. These shapes are generated through the publicly available software called Siris described in Muinonen et al. (1996) and freely available from Muinonen and Nousiainen (2003). To reproduce shapes like the one depicted in Fig. 5 (lower right corner) we chose a power law description of the correlation function. The power law index for the correlation coefficient is set to 3. We chose a minimum polynomial order of 2 and a maximum of 10 (for larger minima the shape has more small scale deformations). Then we vary the relative standard deviation of the radial distance (σ) from 0.02 to 0.5. The generated shapes are represented in Fig. B1 (all simulated intensity patterns are calculated for a fixed size parameter of $x = 46$).

It is clearly seen that for small σ the simulated SID-3 patterns show only slight deviations from the regular concentric rings expected from diffraction theory for a smooth sphere. In contrast, for large deformations (e.g. $\sigma = 0.3$) the patterns show speckles. The larger σ the smaller ~~are~~ the speckle intensity spots in the pattern. The same is also observed for a fixed σ and increasing size parameter (not shown). Thus, σ represents a microphysical shape parameter used to describe the degree of deformation (relative to the smooth sphere). Interestingly, by applying the GLCM method to the simulated patterns, the relative standard deviation of the radial distance (σ) can be related to the normalized energy feature parameter k_{e} (see Fig. B2). A linear relation is obtained between σ and k_{e} up to deformations of about $\sigma = 0.5$ where k_{e} starts to saturate. Although Fig. B2 shows a clear correlation, more such calculations are necessary to investigate the dependence of k_{e} ~~also from the size and the shape of the particles~~on the small-scale complexity of faceted ice crystals. It is envisaged to do these calculations in future with the goal to develop a calibration of the ~~ice~~ small-scale crystal complexity parameter k_{e} against the physical ~~particle~~ ice crystal surface roughness.

Appendix C: Growth rate analysis

In RICE01, the ice particle morphological parameters and their frequencies of occurrence have been measured by the PHIPS imager as functions of temperature, ice saturation ratio (S_{ice}), and pressure. Figure C1 shows an example result for the regrowth experiment RICE01_27 started at an initial temperature of $-50\,^{\circ}\mathrm{C}$. Panel ~~a~~ (a) shows the pressure and temperature inside AIDA during the expansion. The ice saturation ratio S_{ice} is presented in panel ~~b~~(b), and panel ~~c~~ (c) gives the evolution of the particle equivalent diameter during the initial growth (I) and the regrowth (II) phases of the experiment. The AIDA atmospheric conditions forced the generation of two main habit types (compact particles and columns) which could be classified by the imaging system of PHIPS-HALO as well as the replicator strip analysis (Fig. 5). The temporal evolution of the particle equivalent diameters shows quasi linear increases of the particle dimension during the phases of near-constant ice supersaturation conditions (indicated in yellow in Fig. C1). These periods were later used to calculate the particle growth rate. The regrowth at $S_{\text{ice}} \approx 1.2$ (phase II) resulted in the formation of hollow columns that were observed in this phase (sample images in Fig. C1 as well as Fig. 5). In other experiments at higher S_{ice} even more complex deformations were observed due to the fast growth of the crystals. Finally, panel ~~d shows the column/non-column ratio~~ (d) shows the fraction of columnar particles deduced from the PHIPS-HALO images. It shows that the ~~fraction of columnar particles~~ column fraction increased with time, which is due to a size-dependent shape classification for particles in this size range. However, at the final stage of phase II, a column fraction of 0.4 to 0.5 were deduced which is close to 0.58 inferred from the SID-3 patterns analysis. After phase II, there is a period (starting at 1500 s) where the temperature increased and S_{ice} decreased. At this stage the particles started to sublimate at ice subsaturated conditions resulting in the formation of rounded particle edges that could be clearly observed in the PHIPS-HALO images of the columnar ice crystals in this stage (see images in panel ~~c~~ (c) and Fig. 3). Interestingly, the sublimation process results in a scatter of the deduced column fraction in panel ~~d~~(d).

Along a series of AIDA expansions during ~~this campaign~~RICE01, different S_{ice} values were produced at the same temperature to study the influence of S_{ice} on the particle growth rate at constant temperature. The S_{ice} value was kept constant for certain time in each expansion to allow sufficient crystal growth. The growth rates of the ~~c axis, a axis~~c-axis, a-axis, and equivalent diameter of the columnar ice particles were deduced for four different S_{ice} regrowth experiments conducted at the same temperature ($-56\,^{\circ}$C). The results are shown in Fig. C2. In agreement with the results from Bailey and Hallett (2004), the growth rates ~~are proportional to~~ correlate with the ice supersaturation. However, Bailey and Hallett (2004) deduced a linear dependence of the maximum particle dimension with supersaturation while our results rather indicate an exponential dependence. This can be attributed to the ~~difference in experimental procedure where~~ different experimental procedures applied in the two studies. While in the case of Bailey and Hallett (2004), the crystals were nucleated and grown on a glass wire~~while in our case the ice nucleation and growth is contact free~~, the ice particles were nucleated and grown in airborne state in the AIDA cloud chamber, which mimics the formation and growth under natural conditions. It is also noticed that the ~~c axis~~ c-axis grows faster than the ~~a axis~~ a-axis of the columnar ice particles. ~~The~~ However, the c-axis growth rate of 0.047 µm s^{-1} deduced for $S_{\text{ice}} = 1.26$ lies within the range given by Bailey and Hallett (2012) for this saturation ratio.

Acknowledgements. The authors are grateful to all members of the AIDA staff for their continuous support during the chamber experiments. Alexei Kiselev is thanked for producing electron micrographs of ice particle replicas. This work was funded in part by KIT, the German Helmholtz Association, through its research program "Atmosphere and Climate (ATMO)", as well as by the German Research Foundation (DFG) within the HALO priority program 1294 (contract SCHN 1140/1-2) and the research grant SCHN 1140/2-1. The LaMP group would like to acknowledge the EECLAT project (Expecting EarthCare, Learning from A-Train) supported by the French Centre National des Etudes Spatiales (CNES).

The article processing charges for this open-access publication were covered by a Research Centre of the Helmholtz Association.

References

Abdelmonem, A., Schnaiter, M., Amsler, P., Hesse, E., Meyer, J., and Leisner, T.: First correlated measurements of the shape and light scattering properties of cloud particles using the new Particle Habit Imaging and Polar Scattering (PHIPS) probe, Atmos. Meas. Tech., 4, 2125–2142, doi:10.5194/amt-4-2125-2011, 2011.

Abdelmonem, A., Järvinen, E., Duft, D., Hirst, E., Leisner, T., and Schnaiter, M.: PHIPS-HALO: The airborne Particle Habit Imaging and Polar Scattering probe. Part I: Design and Operation, Atmos. Meas. Tech. Discuss., in review, doi:10.5194/amt-2016-42, 2016.

Bailey, M. and Hallett, J.: Growth rates and habits of ice crystals between $-20\,^{\circ}$C and $-70\,^{\circ}$C, J. Atmos. Sci., 61, 514–544, 2004.

Bailey, M. and Hallett, J.: Ice crystal linear growth rates from -20 degrees to -70 degrees C: confirmation from wave cloud studies, J. Atmos. Sci., 69, 390–402, 2012.

Baran, A. J., Havemann, S., Francis, P. N., Watts, P. D.: A consistent set of single-scattering properties for cirrus cloud: tests using radiance measurements from a dual-viewing multi-wavelength satellite-based instrument, J. Quant. Spectrosc. Ra., 79-80, 549–567, doi:10.1016/S0022-4073(02)00307-2 2003.

Baran, A. J., and Francis, P. N.: On the radiative properties of cirrus cloud at solar and thermal wavelengths: A test of model consistency using high-resolution airborne radiance measurements, Q. J. R. Meteorol. Soc., 130, 763–778, doi:10.1256/qj.03.151 2004.

Baran, A. J.: A review of the light scattering properties of cirrus, J. Quant. Spectrosc. Ra., 110, 1239–1260, doi:10.1016/j.jqsrt.2009.02.026, 2009.

Baran, A. J.: From the single-scattering properties of ice crystals to climate prediction: a way forward, Atmos. Res., 112, 45–69, doi:10.1016/j.atmosres.2012.04.010, 2012.

Baran, A. J., Gayet, J.-F., and Shcherbakov, V.: On the interpretation of an unusual in-situ measured ice crystal scattering phase function, Atmos. Chem. Phys., 12, 9355–9364, doi:10.5194/acp-12-9355-2012, 2012.

Baran, A. J., Cotton, R., Furtado, K., Havemann, S., Labonnote, L.-C., Marenco, F., Smith, A., and Thelen, J.-C.: A self-consistent scatteringmodel for cirrus. II: The high and low frequencies, Q. J. R. Meteorol. Soc., 140, 1039–1057, doi:10.1002/qj.2193, 2014

Baran, A. J., Hill, P., Furtado, K., Field, P., and Manners, J.: A Coupled Cloud Physics-Radiation Parameterization of the Bulk Optical Properties of Cirrus and Its Impact on the Met Office Unified

Model Global Atmosphere 5.0 Configuration, J. Climate, 27, 7725–7752, doi:10.1175/JCLI-D-13-00700.1, 2014.

Baran, A. J., Furtado, K., Labonnote, L.-C., Havemann, S., Thelen, J.-C., and Marenco, F.: On the relationship between the scattering phase function of cirrus and the atmospheric state, Atmos. Chem. Phys., 15, 1105–1127, doi:10.5194/acp-15-1105-2015, 2015.

Baum, B. A., Yang, P., Heymsfield, A. J., Schmitt, C. G., Xie, Y., Bansemer, A., Hu, Y. X., and Zhang, Z. B.: Improvements in shortwave bulk scattering and absorption models for the remote sensing of ice clouds, J. Appl. Meteorol. Clim., 50, 1037–1056, 2011.

Bogdan, A.: Reversible formation of glassy water in slowly cooling diluted drops, J. Phys. Chem. B, 110, 12205–12206, doi:10.1021/jp062464a, 2006.

Bogdan, A., Molina, M. J., Sassen, K., and Kulmala, M.: Formation of low-temperature cirrus from H_2SO_4/H_2O aerosol droplets, J. Phys. Chem. A, 110, 12541–12542, doi:10.1029/2003GL017034, 2006.

Bogdan, A., and Molina, M. J.: Why does large relative humidity with respect to ice persist in cirrus ice clouds?, J. Phys. Chem. A, 113, 14123–14130, 2009.

Cole, B. H., Yang, P., Baum, B. A., Riedi, J., and C.-Labonnote, L.: Ice particle habit and surface roughness derived from PARASOL polarization measurements, Atmos. Chem. Phys., 14, 3739–3750, doi:10.5194/acp-14-3739-2014, 2014.

Cotton, R., Osborne, S., Ulanowski, Z., Hirst, E., Kaye, P. H., and Greenaway, R. S.: The ability of the Small Ice Detector (SID-2) to characterize cloud particle and aerosol morphologies obtained during flights of the FAAM BAe-146 research aircraft, J. Atmos. Ocean. Tech., 27, 290–303, doi:10.1175/2009jtecha1282.1, 2010.

Crépel, O., Gayet, J.-F., Fournol, J.-F., and Oshchepkov, S.: A new airborne Polar Nephelometer for the measurement of optical and microphysical cloud properties. Part II: Preliminary tests, Ann. Geophys., 15, 460–470, doi:10.1007/s00585-997-0460-0, 1997.

Ebert, V., Teichert, H., Giesemann, C., Saathoff, H., and Schurath, U.: Fibre-coupled in-situ laser absorption spectrometer for the selective detection of water vapour traces down to the ppb-level, Tech. Mess., 72, 23–30, doi:10.1524/teme.72.1.23.56689, 2005.

Fahey, D. W., Gao, R.-S., Möhler, O., Saathoff, H., Schiller, C., Ebert, V., Krämer, M., Peter, T., Amarouche, N., Avallone, L. M., Bauer, R., Bozóki, Z., Christensen, L. E., Davis, S. M., Durry, G., Dyroff, C., Herman, R. L., Hunsmann, S., Khaykin, S. M., Mackrodt, P., Meyer, J., Smith, J. B., Spelten, N., Troy, R. F., Vömel, H., Wagner, S., and Wienhold, F. G.: The AquaVIT-1 intercomparison of atmospheric water vapor measurement techniques, Atmos. Meas. Tech., 7, 3177–3213, doi:10.5194/amt-7-3177-2014, 2014.

Febvre, G., Gayet, J.-F., Minikin, A., Schlager, H., Shcherbakov, V., Jourdan, O., Busen, R., Fiebig, M., Kärcher, B., and Schumann, U.: On optical and microphysical characteristics of contrails and cirrus, J. Geophys. Res., 114, D02204, doi:10.1029/2008JD010184, 2009.

Field, P. R., Baran, A. J., Kaye, P. H., Hirst, E., and Greenaway, R.: A test of cirrus ice crystal scattering phase functions, Geophys. Res. Lett., 30, 1752–1755, doi:10.1029/2003GL017482, 2003.

Gayet, J. F., Crépel, O., Fournol, J. F., and Oshchepkov, S.: A new airborne polar Nephelometer for the measurements of optical and microphysical cloud properties. Part I: Theoretical design, Ann. Geophys., 15, 451–459, doi:10.1007/s00585-997-0451-1, 1997.

Gayet, J.-F., Auriol, F., Oshchepkov, S., Schroder, F., Duroure, C., Febvre, G., Fournol, J.-F., Crepel, O., Personne, P., and Daugereon, D.: In situ measurements of the scattering phase function of stratocumulus, contrails and cirrus, Geophys. Res. Lett., 25, 971–974, doi:10.1029/98GL00541, 1998.

Gayet, J. F., Ovarlez, J., Shcherbakov, V., Ström, J., Schumann, U., Minikin, A., Auriol, F., Petzold, A., and Monier, M.: Cirrus cloud microphysical and optical properties at southern and northern midlatitudes during the INCA experiment, J. Geophys. Res.-Atmos., 109, 1–13, doi:10.1029/2004JD004803, 2004.

Guignard, A., Stubenrauch, C. J., Baran, A. J., and Armante, R.: Bulk microphysical properties of semi-transparent cirrus from AIRS: a six year global climatology and statistical analysis in synergy with geometrical profiling data from CloudSat-CALIPSO, Atmos. Chem. Phys., 12, 503–525, doi:10.5194/acp-12-503-2012, 2012.

Haag, W., Kärcher, B., Ström, J., Minikin, A., Lohmann, U., Ovarlez, J., and Stohl, A.: Freezing thresholds and cirrus cloud formation mechanisms inferred from in situ measurements of relative humidity, Atmos. Chem. Phys. Discuss., 3, 3267–3299, doi:10.5194/acpd-3-3267-2003, 2003.

Haralick, R. M., Shanmugam, K., and Dinstein, I.: Textural features for image classification, IEEE T. Syst. Man Cyb., SMC-3, 610–621, doi:10.1109/TSMC.1973.4309314, 1973.

Hirst, E., Kaye, P. H., Greenaway, R. S., Field, P., and Johnson, D. W.: Discrimination of micrometre-sized ice and super-cooled droplets in mixed-phase cloud, Atmos. Environ., 35, 33–47, doi:10.1016/S1352-2310(00)00377-0, 2001.

Järvinen, E., Vochezer, P., Möhler, O., and Schnaiter, M.: Laboratory study of microphysical and scattering properties of corona-producing cirrus clouds, Appl. Optics, 53, 7566–7575, 2014.

Johnson, A., Lasher-Trapp, S., Bansemer, A., Ulanowski, Z., and Heymsfield, A. J.: Difficulties in early ice detection with the Small Ice Detector-2 HIAPER (SID-2H) in maritime cumuli, J. Atmos. Ocean. Tech., 31, 1263–1275, doi:10.1175/JTECH-D-13-00079.1, 2014.

Jourdan, O., Oshchepkov, S., and Gayet, J.-F.: Statistical analysis of cloud light scattering and microphysical properties obtained from airborne measurements, J. Geophys. Res., 108, 4155, doi:10.1029/2002JD002723, 2003.

Jourdan, O., Mioche, G., Garrett, T. J., Schwarzenböck, A., Vidot, J., Xie, Y., Shcherbakov, V., Yang, P., and Gayet, J. F.: Coupling of the microphysical and optical properties of an Arctic nimbostratus cloud during the ASTAR 2004 experiment: implications for light-scattering modeling, J. Geophys. Res.-Atmos., 115, D23206, doi:10.1029/2010JD014016, 2010.

Krasinski, M. J., Krasinska, K. R., and Ulanowski, Z.: Investigation of growth kinetics and morphology of sodium fluorosilicate ice-analogue crystals in solutions and gels, Cryst. Res. Technol., 42, 1237–1242, 2007.

Lampert, A., Ehrlich, A., Dörnbrack, A., Jourdan, O., Gayet, J.-F., Mioche, G., Shcherbakov, V., Ritter, C., and Wendisch, M.: Microphysical and radiative characterization of a subvisible midlevel Arctic ice cloud by airborne observations – a case study, Atmos. Chem. Phys., 9, 2647–2661, doi:10.5194/acp-9-2647-2009, 2009.

Liu, C., Yang, P., Minnis, P., Loeb, N., Kato, S., Heymsfield, A., and Schmitt, C.: A two-habit model for the microphysical and optical properties of ice clouds, Atmos. Chem. Phys., 14, 13719–13737, doi:10.5194/acp-14-13719-2014, 2014.

Lu, R.-S., Tian, G.-Y., Gledhill, D., and Ward, S.: Grinding surface roughness measurement based on the co-occurrence matrix of speckle pattern texture, Appl. Optics, 45, 8839, doi:10.1364/ao.45.008839, 2006.

Magee, N. B., Miller, A., Amaral, M., and Cumiskey, A.: Mesoscopic surface roughness of ice crystals pervasive across a wide range of ice crystal conditions, Atmos. Chem. Phys., 14, 12357–12371, doi:10.5194/acp-14-12357-2014, 2014.

Miloshevich, L. M. and Heymsfield, A. J.: A balloon-borne continuous cloud particle replicator for measuring vertical profiles, of cloud microphysical properties: instrument design, performance, and collection efficiency analysis, J. Atmos. Ocean. Tech., 14, 753–768, doi:10.1175/1520-0426(1997)014<0753:ABBCCP>2.0.CO;2, 1997.

Mitchell, D., L., Rasch, P., Ivanova, D., McFarquhar, G., and Nousiainen, T.: Impact of small ice crystal assumptions on ice sedimentation rates in cirrus clouds and GCM simulations, Geophys. Res. Lett., 35, L09806, doi:10.1029/2008GL033552, 2008.

Möhler, O., Büttner, S., Linke, C., Schnaiter, M., Saathoff, H., Stetzer, O., Wagner, R., Krämer, M., Mangold, A., Ebert, V., and Schurath, U.: Effect of sulfuric acid coating on heterogeneous ice nucleation by soot aerosol particles, J. Geophys. Res., 110, D11210, doi:10.1029/2004jd005169, 2005a.

Möhler, O., Linke, C., Saathoff, H., Schnaiter, M., Wagner, R., Mangold, A., Krämer, M., and Schurath, U.: Ice nucleation on flame soot aerosol of different organic carbon content, Meteorol. Z, 14, 477–484, 2005b.

Möhler, O., Field, P. R., Connolly, P., Benz, S., Saathoff, H., Schnaiter, M., Wagner, R., Cotton, R., Krämer, M., Mangold, A., and Heymsfield, A. J.: Efficiency of the deposition mode ice nucleation on mineral dust particles, Atmos. Chem. Phys., 6, 3007–3021, doi:10.5194/acp-6-3007-2006, 2006.

Muinonen, K. and Nousiainen, T.: Free software for light scattering by small particles, available at: https://wiki.helsinki.fi/display/PSR/SIRIS (last access: 3 November 2015), 2003.

Muinonen, K., Nousiainen, T., Fast, P., Lumme, K., and Peltoniemi, J. I.: Light scattering by Gaussian random particles: ray optics approximation, J. Quant. Spectrosc. Ra., 55, 577–601, doi:10.1016/0022-4073(96)00003-9, 1996.

Murphy, D. M. and Koop, T.: Review of the vapour pressures of ice and supercooled water for atmospheric applications, Q. J. Roy. Meteor. Soc., 131, 1539–1565, doi:10.1256/qj.04.94, 2005.

Neshyba, S. P., Lowen, B., Benning, M., Lawson, A., and Rowe, P. M.: Roughness metrics of prismatic facets of ice, J. Geophys. Res., 118, 3309–3318, 2013.

Oshchepkov, S., Isaka, H., Gayet, J.-F., Sinyuk, A., Auriol, F., Havemann, S.: Microphysical properties of mixed-phase & ice clouds retrieved from in situ airborne "Polar Nephelometer" measurement, Geophys. Res. Lett., 27, 209–212, 2000

Pfalzgraff, W. C., Hulscher, R. M., and Neshyba, S. P.: Scanning electron microscopy and molecular dynamics of surfaces of growing and ablating hexagonal ice crystals, Atmos. Chem. Phys., 10, 2927–2935, doi:10.5194/acp-10-2927-2010, 2010.

Schmitt, C. G. and Heymsfield, A. J.: Observational quantification of the separation of simple and complex atmospheric ice particles, Geophys. Res. Lett., 41, 1301–1307, doi:10.1002/2013GL058781, 2014.

Schnaiter, M., Kaye, P. H., Hirst, E., Ulanowski, Z., and Wagner, R.: Exploring the surface roughness of small ice crystals by measuring high resolution angular scattering patterns, AAPP, Phys. Math. Nat. Sci., 89, C1V89S1P084, doi:10.1478/C1V89S1P084, 2011.

Schnaiter, M., Büttner, S., Möhler, O., Skrotzki, J., Vragel, M., and Wagner, R.: Influence of particle size and shape on the backscattering linear depolarisation ratio of small ice crystals – cloud chamber measurements in the context of contrail and cirrus microphysics, Atmos. Chem. Phys., 12, 10465–10484, doi:10.5194/acp-12-10465-2012, 2012.

Schön, R., Schnaiter, M., Ulanowski, Z., Schmitt, C., Benz, S., Möhler, O., Vogt, S., Wagner, R., and Schurath, U.: Particle habit imaging using incoherent light: a first step toward a novel instrument for cloud microphysics, J. Atmos. Ocean. Tech., 28, 493–512, 2011.

Seifert, M., Tiede, R., Schnaiter, M., Linke, C., Mohler, O., Schurath, U., and Strom, J.: Operation and performance of a differential mobility particle sizer and a TSI 3010 condensation particle counter at stratospheric temperatures and pressures, J. Aerosol Sci., 35, 981–993, 2004.

Ström, J., Seifert, M., Kärcher, B., Ovarlez, J., Minikin, A., Gayet, J.-F., Krejci, R., Petzold, A., Auriol, F., Haag, W., Busen, R., Schumann, U., and Hansson, H. C.: Cirrus cloud occurrence as function of ambient relative humidity: a comparison of observations obtained during the INCA experiment, Atmos. Chem. Phys., 3, 1807–1816, doi:10.5194/acp-3-1807-2003, 2003.

Takahashi, T. and Fukuta, N.: Ice crystal replication with common plastic solutions, J. Atmos. Ocean. Tech., 5, 129–135, doi:10.1175/1520-0426(1988)005<0129:ICRWCP>2.0.CO;2, 1988.

Tricoli, U., Vochezer, P., and Pfeilsticker, K.: Transition operator calculation with Green's dyadic technique for electromagnetic scattering: a numerical approach using the Dyson equation, J. Quant. Spectrosc. Ra., 162, 77–88, doi:10.1016/j.jqsrt.2015.04.006, 2015.

Ulanowski, Z., Hesse, E., Kaye, P. H., Baran, A. J., and Chandrasekhar, R.: Scattering of light from atmospheric ice analogues, J. Quant. Spectrosc. Ra., 79, 1091–1102, 2003.

Ulanowski, Z., Hesse, E., Kaye, P. H., and Baran, A. J.: Light scattering by complex ice-analogue crystals, J. Quant. Spectrosc. Ra., 100, 382–392, 2006.

Ulanowski, Z., Kaye, P. H., Hirst, E., and Greenaway, R.: Light scattering by ice particles in the Earth's atmosphere and related laboratory measurements, in: Electromagn. Light Scatt. XII, Conf. Proceedings, edited by: Muinonen, K., Penttilä, A., Lindqvist, H., Nousiainen, T., and Videen, G., 28 June–2 July 2010, Univ. Helsinki, Finl., 294–297, 2010.

Ulanowski, Z., Kaye, P. H., Hirst, E., Greenaway, R. S., Cotton, R. J., Hesse, E., and Collier, C. T.: Incidence of rough and irregular atmospheric ice particles from Small Ice Detector 3 measurements, Atmos. Chem. Phys., 14, 1649–1662, doi:10.5194/acp-14-1649-2014, 2014.

van Diedenhoven, B., Cairns, B., Fridlind, A. M., Ackerman, A. S., and Garrett, T. J.: Remote sensing of ice crystal asymmetry parameter using multi-directional polarization measurements –

Part 2: Application to the Research Scanning Polarimeter, Atmos. Chem. Phys., 13, 3185–3203, doi:10.5194/acp-13-3185-2013, 2013.

Vochezer, P., Järvinen, E., Wagner, R., Kupiszewski, P., Leisner, T., and Schnaiter, M.: In situ characterization of mixed phase clouds using the Small Ice Detector and the Particle Phase Discriminator, Atmos. Meas. Tech.~~Discuss., 8, 6511–6558~~, 9, 159–177, doi:~~10.5194/amtd-8-6511-2015, 2015.~~ 10.5194/amt-9-159-2016, 2016.

Wagner, R., Bunz, H., Linke, C., Möhler, O., Naumann, K. H., Saathoff, H., Schnaiter, M., and Schurath, U.: Chamber simulations of cloud chemistry: the AIDA Chamber, in: NATO Adv. Res. Work. Environ. Simul. Chambers Appl. to Atmos. Chem. Process. (2004 Zakopane, Poland), edited by: Barnes, I., and Rudzinski, K. J., Springer, Dordrecht, the Netherlands, 2006.

Wagner, R., Benz, S., Bunz, H., Möhler, O., Saathoff, H., Schnaiter, M., Leisner, T., and Ebert, V.: Infrared optical constants of highly diluted sulfuric acid solution droplets at cirrus temperatures, J. Phys. Chem. A, 112, 11661–11676, 2008.

Wagner, R., Möhler, O., Saathoff, H., Schnaiter, M., and Leisner, T.: High variability of the heterogeneous ice nucleation potential of oxalic acid dihydrate and sodium oxalate, Atmos. Chem. Phys., 10, 7617–7641, doi:10.5194/acp-10-7617-2010, 2010.

Wagner, R., Höhler, K., Möhler, O., Saathoff, H., and Schnaiter, M.: Crystallization and immersion freezing ability of oxalic and succinic acid in multi-component aqueous organic aerosol particles, Geophys. Res. Lett., 42, 2464–2472, doi:10.1002/2015GL063075, 2015.

Yang, H., Dobbie, S., Herbert, R., Connolly, P., Gallagher, M., Ghosh, S., Al-Jumur, S. M. R. K., and Clayton, J.: The effect of observed vertical structure, habits, and size distributions on the solar radiative properties and cloud evolution of cirrus clouds, Q. J. R. Meteorol. Soc., 138, 1221–1232, doi:10.1002/qj.973, 2012.

Yang, P., Liou, K.-N., Bi, L., Liu, C., Yi, B., and Baum, B. A.: On the radiative properties of ice clouds: Light scattering, remote sensing, and radiation parameterization, Adv. Atmos. Sci., 32, 32–63, doi:10.1007/s00376-014-0011-z, 2015.

Yi, B., Yang, P., Baum, B. A., L'Ecuyer, T., Oreopoulos, L., Mlawer, E. J., Heymsfield, A. J., and Liou, K.-N.: Influence of ice particle surface roughening on the global cloud radiative effect, J. Atmos. Sci., 70, 2794–2807, doi:10.1175/JAS-D-13-020.1, 2013.

Yurkin, M. and Hoekstra, A.: User manual for the discrete dipole approximation code ADDA 1.1, available at: http://a-dda.googlecode.com/svn/tags/rel_1.1/doc/manual.pdf (last access: 3 November 2015), 2012.

Zhang, Y., Macke, A., and Albers, F.: Effect of crystal size spectrum and crystal shape on stratiform cirrus radiative forcing, Atmos. Res., 52, 59–75, 1999.

Table 1. Results of the particle fraction analysis for those experiments of the RICE01 and RICE03 campaign that are respectively labelled in blue and red in Figs. 4 and 6. All experiments where conducted at an initial temperature of $-50\,^{\circ}\mathrm{C}$ and with soot particles as heterogeneous ice nuclei.

Exp.	S_{ice}	$\xi_{\mathrm{v}}^{\mathrm{acw}}$ [ppmv]	Fraction of rough particles	Fraction of columns	Fraction of rough columns*	Fraction of halo crystals
			RICE01			
22	1.02	0.86	0.14	0.63	0.06	0.34
23	1.14	3.97	0.44	0.65	0.28	0.39
24	1.25	6.71	0.60	0.56	0.41	0.37
26	1.38	10.6	0.84	0.39	0.73	0.31
			RICE03			
40	1.13	4.48	0.51	0.58	0.24	0.41
42	1.30	7.03	0.72	0.45	0.50	0.22
43	1.20	4.33	0.55	0.53	0.28	0.29

* Ratio of the number of rough columns to the number of all columns.

Table A1. Relative 1σ standard deviations of the three GLCM features k_e, energy E, and combined roughness. The SID-3 patterns were acquired on the analogue ice particle shown in Fig. A1. The GLCM speckle texture analysis was restricted to three different grey-level ranges.

Grey-level range	k_e	Energy E	Combined roughness
10–25	0.66 %	1.38 %	0.95 %
10–50	0.49 %	5.48 %	1.43 %
1–100	0.72 %	7.77 %	1.79 %

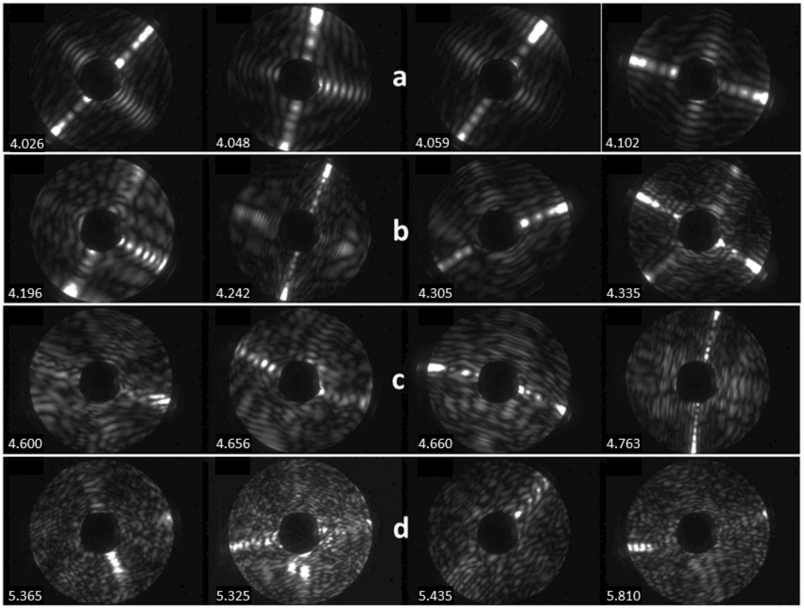

Figure 1. Representative examples of 2-D light scattering patterns of individual small columnar ice particles generated in re-growth cloud chamber experiments at $-50\,^{\circ}$C. The patterns are labelled by the ~~image texture feature energy (upper left corner) and~~ energy feature parameter k_{e} (lower left corner). The patterns are arranged according to increasing k_{e} from left to right and from panel **(a)** to panel **(d)**. ~~Rough particle~~ Particle fractions that have a significant degree of small-scale complexity are deduced by setting a threshold value of $k_{\mathrm{e}}^{\mathrm{thr}} = 4.6$ and classifying all particles equal and above as ~~rough~~complex.

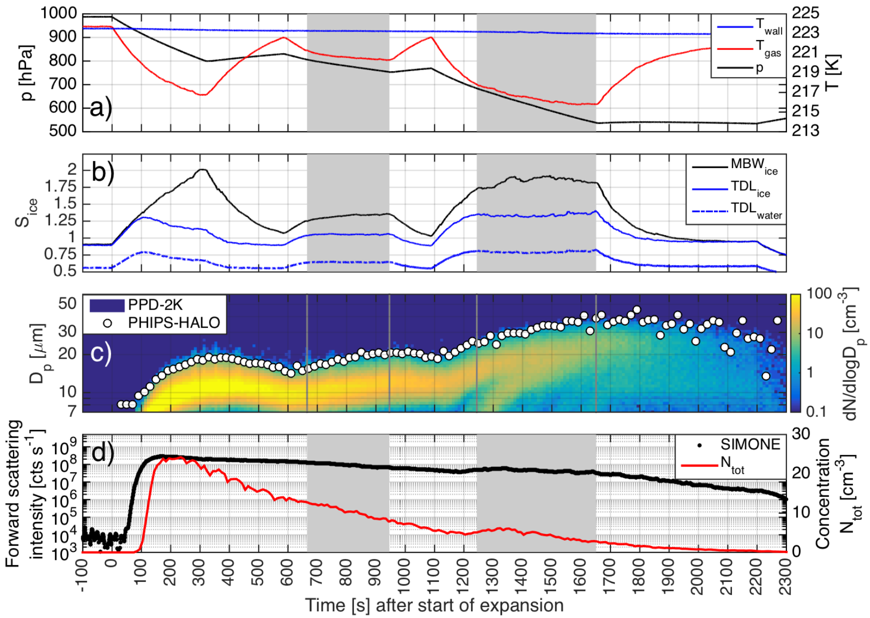

Figure 2. Example of a regrowth experiment conducted in the AIDA cloud chamber at an initial temperature of $-50\,^{\circ}$C. The experimental procedure is specifically designed to grow and sublimate ice particles at defined super- and subsaturated ice conditions (solid blue line in panel **b**). Regrowth periods are indicated by the shaded areas. See text for details.

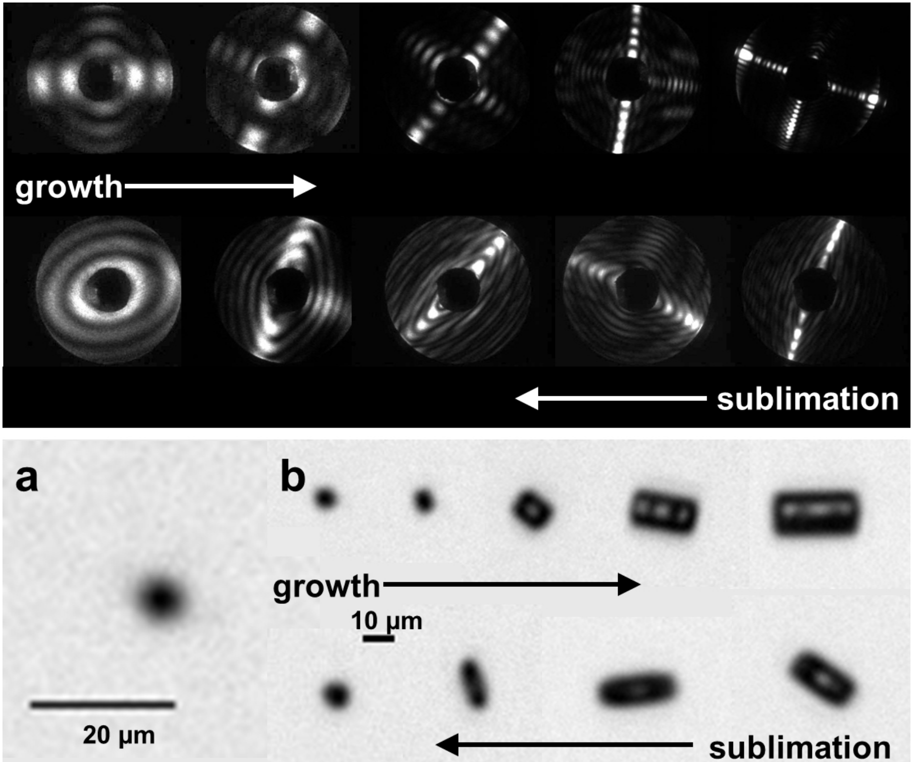

Figure 3. Evolution of SID-3 scattering patterns (upper panel) and PHIPS-HALO micrographs (series b in the lower panel) of columnar ice particles collected during growth and sublimation periods in the $-40\,^{\circ}$C temperature range. Ice particle surface processing by sublimation is clearly visible by a roundening of the ice particle edges resulting in oval SID-3 scattering patterns. Note that SID-3 is capable to determine the particle shape for crystals with sizes of only 2 to 3 µm (patterns on the left side of the upper panel) whereas the imaging method used in PHIPS-HALO cannot give a clear shape information for particles smaller than about 10 µm (image a in the lower panel).

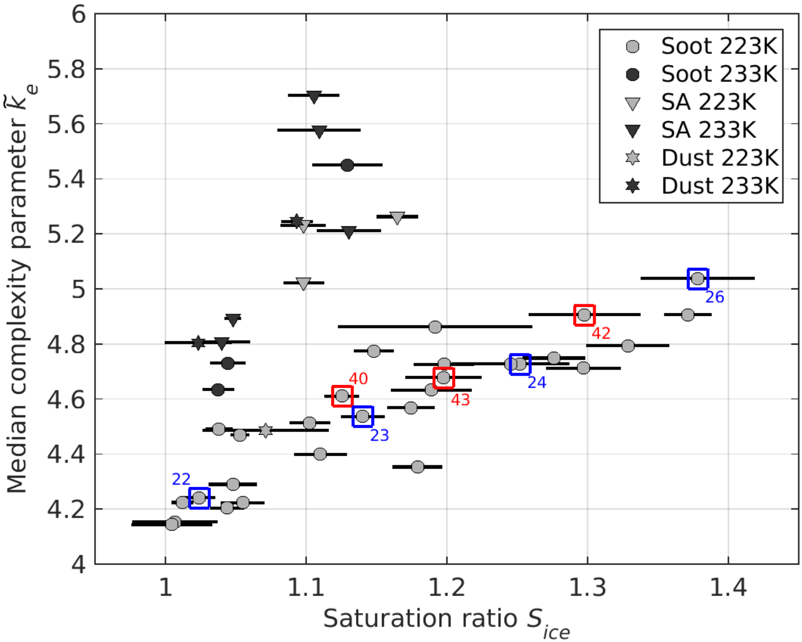

Figure 4. Median ice crystal complexity parameter $\widetilde{k}_e$ deduced from SID-3 scattering patterns that were measured in simulated cirrus clouds at the AIDA cloud chamber. The ice clouds were grown at different ice saturation ratios S_{ice} and at initial chamber temperatures of $-40\,^\circ$C (black symbols) and $-50\,^\circ$C (grey symbols). Three different aerosol types were used to nucleate ice by heterogeneous nucleation on soot (circles) and mineral dust (stars) as well as by homogeneous nucleation in aqueous sulfuric acid particles (triangles).

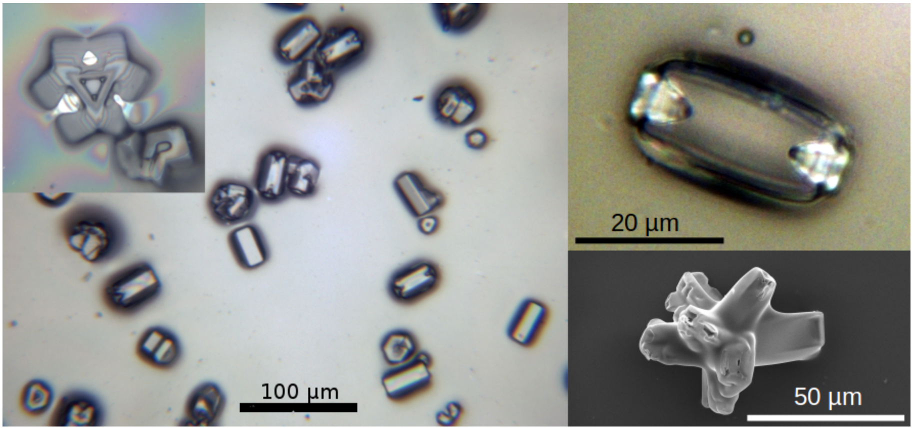

Figure 5. Ice particle replicas generated in the regrowth period of RICE01_27 at a temperature around $-55\,^{\circ}\mathrm{C}$ and an ice supersaturation of 19 %. The particle habit distribution is a mixture of solid and hollow columns as well as small rosettes (left). Hollow rosette with a maximum dimension of about 35 µm (upper left). ~~Stepped hollow column as observed occasionally~~ Although stepped hollowness is difficult to see with the replication method on small ice crystals, it can be identified in cases when the ice particle was ideally replicated (upper right image). Scanning electron micrograph of a rosette replica showing that in general the ice particle surface properties (including stepped hollowness) are masked by the Formvar replication method (lower right).

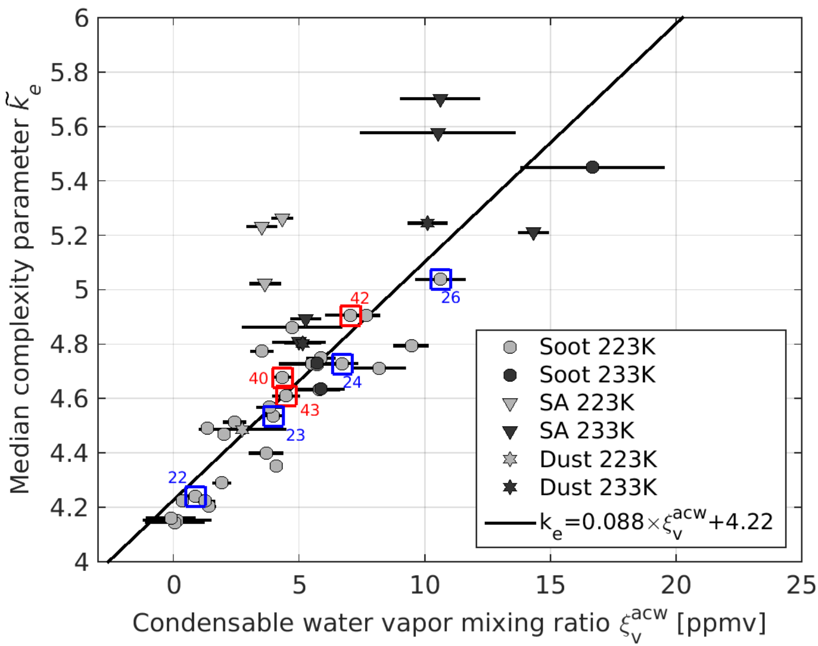

Figure 6. Median ice crystal complexity parameter $\widetilde{k}_e$ plotted against the condensable water vapour mixing ratio that was available during the regrowth of the ice particles.

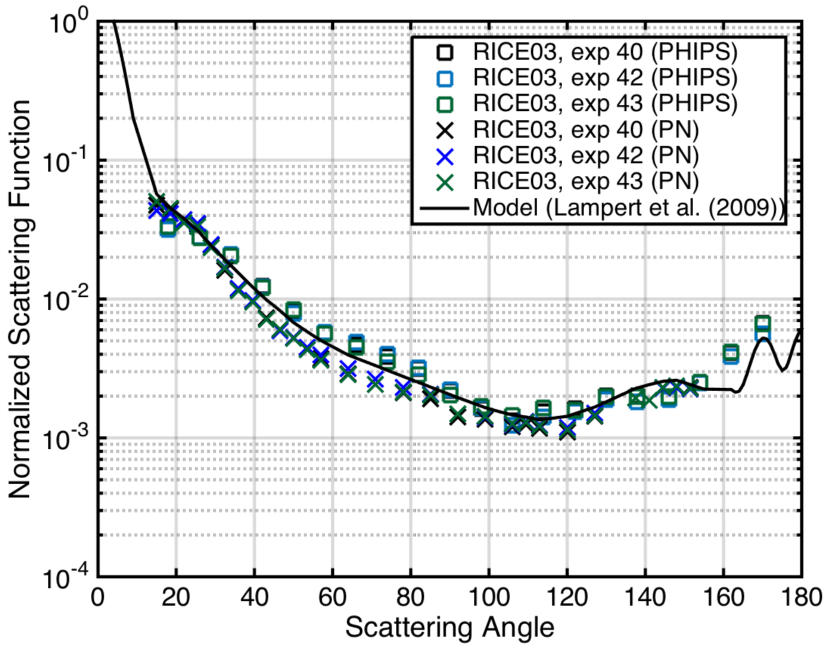

Figure 7. Mean angular scattering functions measured in the regrowth periods of those ice cloud experiments of RICE03 that are labelled in red in Figs. 4 and 6. Two polar nephelometers were deployed in these experiments; the airborne approved polar nephelometer from Clermont-Ferrand (PN, crosses) and the novel instrument PHIPS-HALO from KIT (squares).

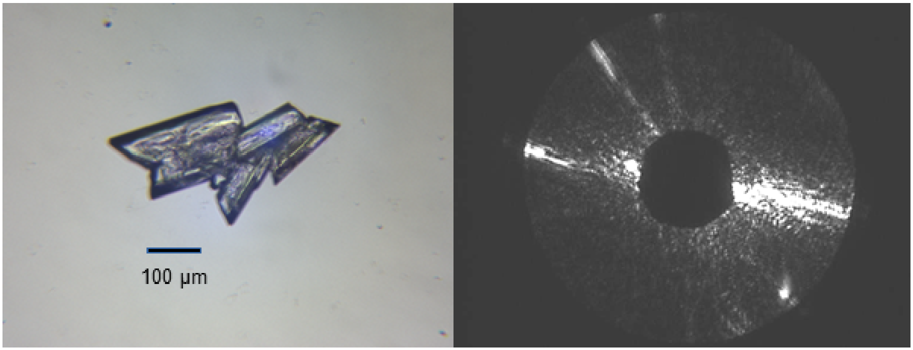

Figure A1. Microscopic image of an ice analogue aggregate with rough surface residing on a poly-carbonate window (left). The sodium fluorosilicate crystals can grow to hexagonal morphologies similar to water ice crystals. The fact that their refractive index is close to water ice makes them well suited for light scattering investigations (Ulanowski et al., 2003, 2006). The crystal was moved into the sensitive area of SID-3 where scattering ~~patters~~ patterns were acquired (right).

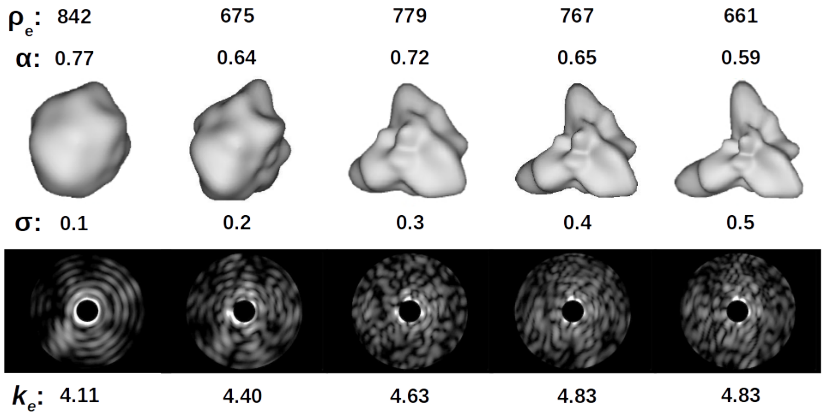

Figure B1. Distorted spherical ice model particles with different deformation ~~parameter~~ parameters σ, effective densities ρ_e, and area ratios α that were used in the ADDA/GDT-matrix approach (upper panel). All input model particles have a fixed size parameter of 46. Corresponding 8 bit grey-scale output patterns (lower panel). The k_e values of the GLCM ~~pattern~~ analysis are given below each pattern.

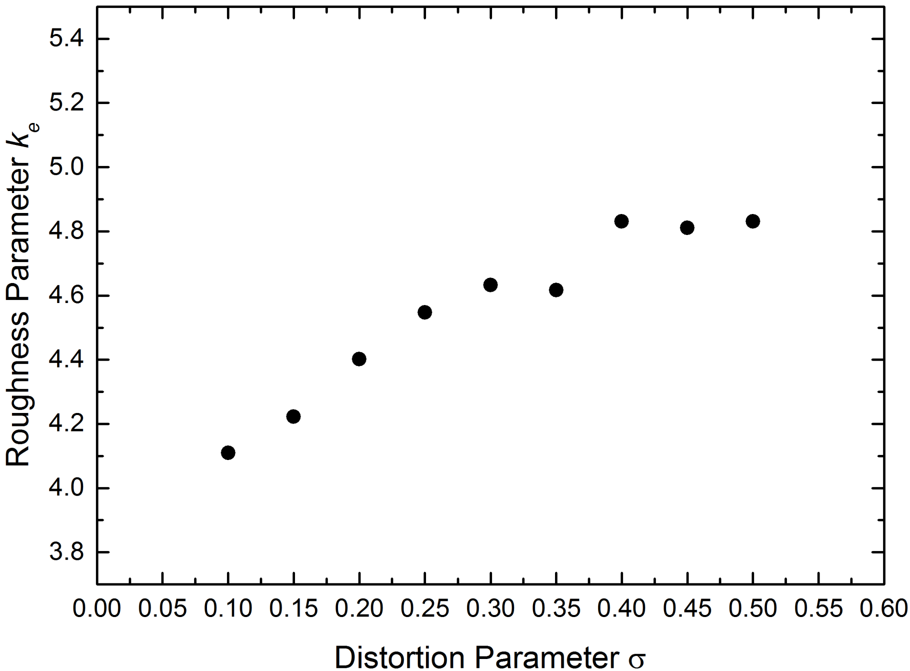

Figure B2. Dependence of the crystal complexity parameter k_e on the distortion parameter σ for the model particles shown in Fig. B1.

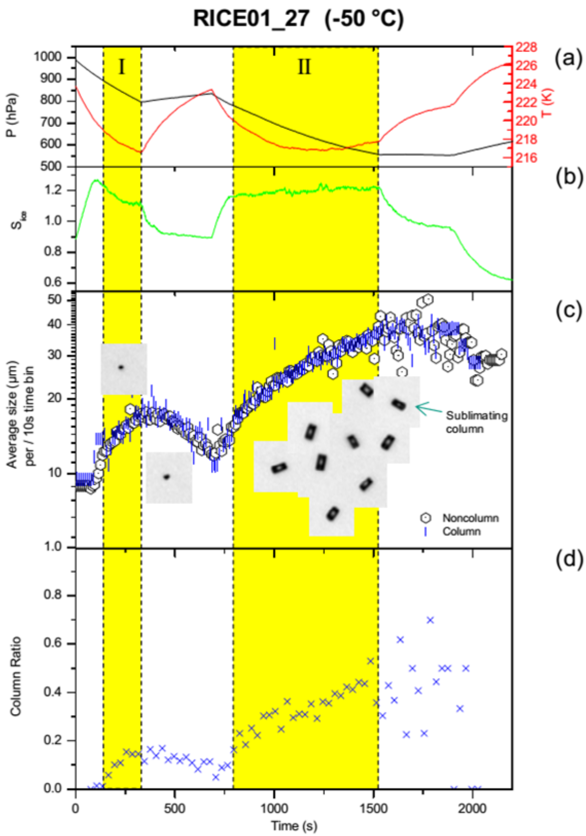

Figure C1. Temporal evolution of the AIDA cirrus cloud experiment RICE01_27. **(a)** Gas temperature and pressure inside the AIDA chamber. **(b)** Ice saturation ratio S_{ice} inside the AIDA volume. **(c)** Geometric particle diameters as measured by PHIPS-HALO. **(d)** Column ratio during the experiment.

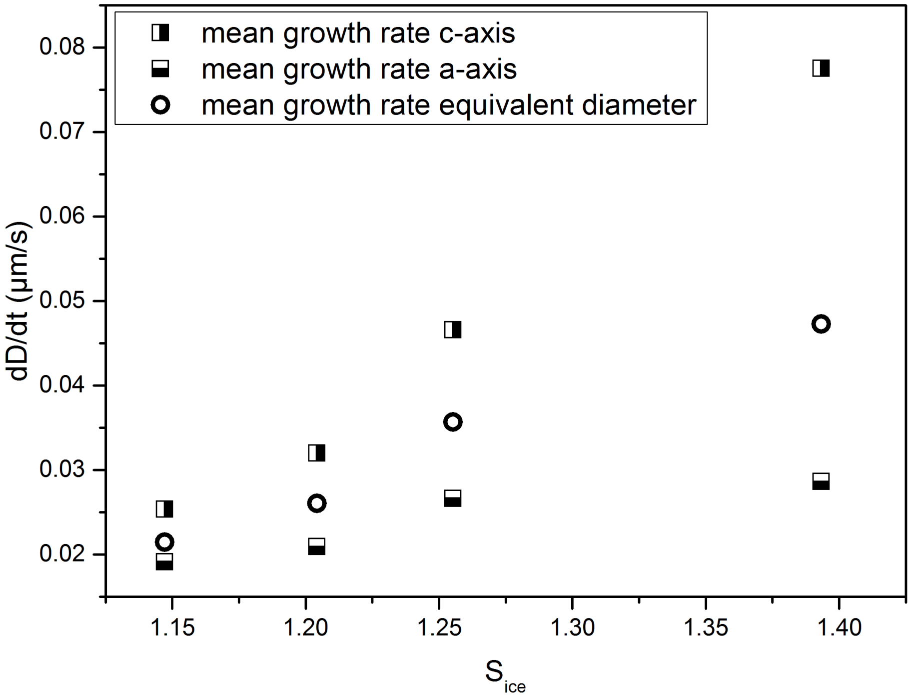

Figure C2. Growth rates of the ~~c axis~~c-axis, ~~a axis~~a-axis, and equivalent diameter of columnar ice particles deduced for four different S_{ice} regrowth experiments. The regrowth periods were conducted at the same temperature of $-56\,^{\circ}$C.